Thesis for the Degree of Licentiate of Engineering

Point processes and convex sets - applications in fatigue

Jenny Andersson

CHALMERS | GÖTEBORG UNIVERSITY

Department of Mathematical Statistics
Chalmers University of Technology and Göteborg University
SE-412 96 Göteborg, Sweden
Göteborg, Sweden 2003

Point processes and convex sets - applications in fatigue
Jenny Andersson

ISSN 0347-2809/No 2003:64
Department of Mathematical Statistics
Chalmers University of Technology and Göteborg University
SE-412 96 Göteborg, Sweden
Telephone +46 (0)31-772 1000
Göteborg, 2003

Point processes and convex sets - applications in fatigue
Jenny Andersson
Department of Mathematical Statistics
Chalmers University of Technology and Göteborg University

Abstract

Two modelling approaches from stochastic geometry, that can be applied to fatigue problems, are introduced.

First, the grain structure of the surface of a metal is modelled as a Voronoi tessellation of Poisson points in the plane. As an example of this approach, we study the influence of grain structure on fatigue life. A crack growth model is applied to simulated grain structures. The conclusion is that the fatigue life decreases, compared to a model with grains of equal size. Also the life variation, due to the random grain structure, can be estimated.

The second approach is to describe inclusions in steel by two models of non-overlapping convex sets, which are generalisations of Matérn's hard-core models. In both cases, we start with a Poisson process and assign a convex set to each point. The point process is then thinned so that no set intersects another set. We derive the second-order product density for convex sets with the same orientation. The product density can be used to compare the models to a homogeneous Poisson process. For spherical sets of equal radii, there can be no point within a distance of less than two times the radius to another point. Pairs of points at distances between two and four times the radius are more frequent than in a Poisson process. For larger distances the frequency of point pairs is the same as for a Poisson process.

Keywords: Poisson process; Convex sets; Material fatigue; Voronoi tessellation; Germ-grain process; Second-order measures; Short cracks

Acknowledgements

There are a number of people who consciously or not have helped me with this thesis. In particular I want to thank:

Jacques de Maré, for being my supervisor through this work and patiently reading the manuscript and above all raising constructive questions. In addition, I am tremendously grateful for being led back on track after a detour into chemical engineering.

Thomas Svensson, for supervising the first part of this work, especially for helping out with problems related to fatigue.

Marianne Månsson, my supervisor for the second part of this work, for always being ready to discuss my questions regarding point processes and for being thoroughly involved in my problem.

Holger Rootzén, my first-year supervisor, in particular for many useful comments about writing and doing presentations.

Everyone at Mathematical Statistics, for providing an inspiring and friendly atmosphere.

My parents and my brother, for encouragement and support.

Johan, for being lovely.

Contents

List of papers

This thesis consists of the following papers

Paper A J. Andersson *The influence of grain size variation on metal fatigue*, submitted for publication.

Paper B J. Andersson *Product densities of two models of non-overlapping grains.*

1 Introduction

Stochastic geometry has many applications in the physical sciences. In this licentiate thesis, we will focus on two problems in fatigue. In fatigue, the structure of the material considered, is crucial. We will describe the characteristics of two types of materials, on two different scales, by means of convex sets associated with the points of a point process.

The literature on applications of stochastic geometry is extensive. We will not attempt to make a detailed reference list here, but instead give [8] as an excellent starting point. A survey on the applications of Voronoi tessellations can be found in [7]. Stochastic models suitable for modelling materials are described in [2].

The first paper, Paper A, appended to this thesis, uses a Voronoi tessellation on Poisson points as the grain structure of a metal without defects. The influence of grain structure on fatigue life is then studied by simulating such grain structures and letting a crack grow according to a deterministic crack growth model.

The second paper, Paper B, is more mathematical. Important defects present in some materials, particularly in steel, are inclusions. Those inclusions, see Figure 1, can consist of, for example, sulphides or oxides and are often approximately spherical. In this paper we calculate a second-order characteristic of two models for such inclusions in metals. The two models are examples of point processes of non-overlapping convex sets. A special case is when the convex sets are spheres.

The outline of this thesis is as follows. Some background for the appended papers is given in Sections 2, 3 and 4. First, we give an introduction to point processes, followed by a short description of fatigue and finally a section on the structures of metals. In Sections 5 and 6 there are summaries of Papers A and B respectively. Note that the word grain has different meanings in the two papers. In Paper A a grain is a part of the metal with equal orientation of the atom layers. In Paper B the non-overlapping sets are called grains in accordance with such models usually being called germ-grain models. Finally, some conclusions and ideas for further work are given in Section 7.

2 Stochastic geometry

We start with the definition of a point process and continue with some basic definitions to make the notation clear. Let N be the family of all sequences, ϕ, of points in $\mathbb{R}^d$ such that ϕ is locally finite, that is each bounded subset of $\mathbb{R}^d$ contains a finite number of points of ϕ. Usually ϕ is also required to be simple, that is all points of ϕ are distinct. If B is a subset of $\mathbb{R}^d$ denote

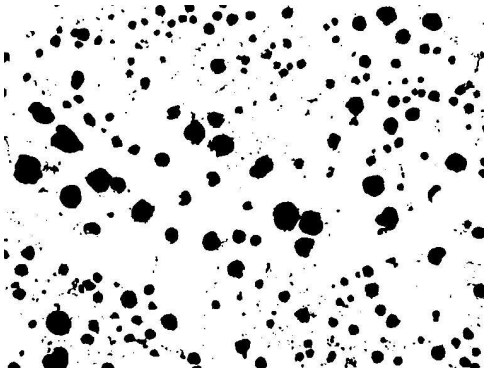

Figure 1: A cut of cast iron with the black shapes being defects. The image was produced by Stefano Beretta.

the number of points of ϕ in B by $\phi(B)$. Let $\mathcal{N}$ be the smallest σ-algebra on N such that all mappings $\phi \to \phi(B)$ are measurable for any Borel set B. The formal definition of a *point process* Φ in $\mathbb{R}^d$ is as a measurable mapping of a probability space $(\Omega, \mathcal{F}, \mathbb{P})$ into $(N, \mathcal{N})$.

The *distribution*, P, of a point process Φ is defined as

$$P(Y) = \mathbb{P}(\Phi \in Y) = \mathbb{P}(\{\omega \in \Omega : \Phi(\omega) \in Y\}), \quad Y \in \mathcal{N}.$$

The *expectation* of the number of points of Φ in a set B can be written

$$\mathbb{E}[\Phi(B)] = \int_N \phi(B) P(\mathrm{d}\phi) = \mathbb{E}\left[\sum_{x \in \Phi} 1_B(x)\right].$$

A point process Φ is *stationary* if its distribution is invariant under translation, that is the processes $\Phi = \{X_n\}$ and $\Phi_x = \{X_n + x\}$ have the same distribution for all $x \in \mathbb{R}^d$. Furthermore it is *isotropic* if its distribution is invariant under rotations about the origin. The *intensity measure* Λ of Φ is defined as

$$\Lambda(B) = \mathbb{E}[\Phi(B)],$$

for B a Borel set. If it has density with respect to Lebesgue measure then Λ can be written in terms of an *intensity function* $\lambda(x)$,

$$\Lambda(B) = \int_B \lambda(x) \mathrm{d}x.$$

If the process is stationary, the intensity function is independent of x and it becomes a non-negative real constant, called the *intensity*, λ. Let the Lebesgue measure in $\mathbb{R}^d$ be denoted l_d and then for a stationary process

$$\Lambda(B) = \lambda l_d(B).$$

A useful theorem, which will be applied in a more complicated form in Paper B, is the Campbell theorem. For any non-negative measurable function f,

$$\mathbb{E}\left[\sum_{x\in\Phi} f(x)\right] = \int \sum_{x\in\phi} f(x)P(\mathrm{d}\phi) = \int f(x)\Lambda(\mathrm{d}x).$$

In the stationary case the last expression is simplified to

$$\lambda \int f(x)\mathrm{d}x.$$

Corresponding to variances and covariances of stochastic variables are the second-order measures of a point process. One such measure is the *second-order factorial moment measure* $\alpha^{(2)}$, defined on $\mathbb{R}^d \times \mathbb{R}^d$. If B_1 and B_2 are Borel sets and Φ is a point process on $\mathbb{R}^d$ with distribution P, $\alpha^{(2)}$ is defined as

$$\begin{aligned}\alpha^{(2)}(B_1 \times B_2) =& \mathbb{E}[\#\{(x,y) : x \in \Phi \cap B_1, y \in \Phi \cap B_2, x \neq y\}] \\ =& \int \sum_{\substack{x_1,x_2\in\phi \\ x_1\neq x_2}} 1_{B_1}(x_1)1_{B_2}(x_2)P(\mathrm{d}\phi).\end{aligned}$$

For a stationary Poisson process with intensity λ it is equal to $\lambda^2 l_d(B_1)l_d(B_2)$. If the second-order factorial moment measure $\alpha^{(2)}$ has density with respect to the Lebesgue measure, this density is called the *second-order product density* $\varrho^{(2)}$. An interpretation of the second-order product density is that $\varrho^{(2)}(x,y)dV_1dV_2$ is the probability of having a point in each of two infinitesimally small disjoint Borel sets, with Lebesgue measures dV_1 and dV_2, where x and y belong to one set each.

The *variance* of the number of points in a Borel set B can be written in terms of $\alpha^{(2)}$ as

$$\mathrm{Var}(\Phi(B)) = \alpha^{(2)}(B \times B) + \Lambda(B) - \Lambda(B)^2.$$

If B_1 and B_2 are Borel sets, the *covariance* of the number of points in these two sets is,

$$\mathrm{Cov}(\Phi(B_1), \Phi(B_2) = \alpha^{(2)}(B_1 \times B_2) + \Lambda(B_1 \cap B_2) - \Lambda(B_1)\Lambda(B_2).$$

A *marked point process* on $\mathbb{R}^d$, $\Psi = \{X_n, M_n\}$, is a point process in $\mathbb{R}^d$, with points X_n, each having a mark M_n belonging to some space of marks, M. The marked process can be interpreted as an ordinary point process on the space $\mathbb{R}^d \times M$. Every definition for ordinary point processes can be repeated analogously for marked processes. The only difference is that a translation of a marked process usually only acts on the points and not on the marks.

A *tessellation* partitions an Euclidean space, $\mathbb{R}^d$, into sets, C_i, with non-overlapping interior, that is $\mathbb{R}^d = \cup_i C_i$. Let $\{p_i\}$ be a set of points. Each point p_i in this set, from now on called nucleus, generates a cell (or grain) C_i. Let one grain C_i consist of all points in $\mathbb{R}^d$ which has p_i as their nearest nucleus,

$$C_i = \{x \in \mathbb{R}^d : \|p_i - x\| \leq \|p_j - x\| \ , \forall p_j\}, \tag{1}$$

where $\|\cdot\|$ is the Euclidean distance. If the set of points, $\{p_i\}$, is locally finite, i.e. any finite region contains a finite number of points, the C_i's are called a *Voronoi tessellation* and C_i a Voronoi cell.

See [8] for a general reference on point processes. A general reference on the properties of Voronoi tessellations is [7] and a more mathematical one is [5].

3 Fatigue

Fatigue is the failure in a structure that occurs after the structure has been subjected to a repeated load. The term fatigue is used since the failure often occurs after a long period of repeated stress, at a level considerably lower than the stress needed to break the structure if it was applied only once. The standard example of fatigue is to take a paperclip and notice that it breaks after repeatedly bending it back and forth at the same spot, although it is virtually impossible to break it in one bending. When a metal is subjected to a load, it is possible that small cracks start to form in the metal grains, most often at the surface. Cracks can also start growing in some defect already present within the metal. The cracks then continue to grow, as more load cycles are applied, until a crack spans the entire object and it breaks. Possibly cracks can stop or close, but that is not our concern here.

To assess the fatigue properties of materials, laboratory tests can be performed. Identical test specimens are subjected to a cyclic load until the specimens break or to a maximum number of load cycles. The procedure is repeated for different load amplitudes. Data are plotted in a Wöhler curve, where the logarithm of the load amplitude is plotted against the logarithm

of the number of cycles to failure. Often there is a linear relation between the load level and the fatigue life, the number of cycles to failure, for high loads. For some materials there may be a fatigue limit, that is a stress level below which failure will never occur. In [1] there is a section on fatigue.

4 Metal structure

Metals are crystalline materials, that is the atoms are ordered in a three-dimensional pattern. Common atomic arrangements in metals are the body-centred cubic (BCC), the face-centred cubic (FCC) and the hexagonal closed-packed (HCP) structures. The last two arrangements are the most efficient ways, in terms of occupied space, of stacking equally sized spheres and because of this they are called close-packed structures. One way of illustrating the atomic structure is in terms of a unit cell, which is the smallest repetitive unit within the crystal, see Figure 2.

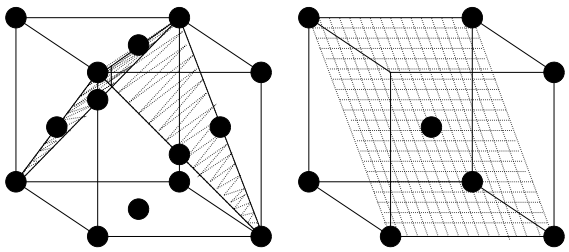

Figure 2: Unit cells of the face-centred cubic (to the left) and the body-centred cubic atomic structures. Two slip planes are shaded in the FCC cell and one in the BCC cell.

A slip plane, such as those shown in Figure 2, is a preferred plane of atoms that will move when a stress is applied. The number of unique non-parallel slip planes depends on the crystal structure. The FCC crystal has four slip planes, the BCC has six and the HCP has one. Each plane can slip in three directions in the FCC and HCP crystals and in two directions in the BCC crystal.

A crystalline material is usually composed of many crystals. In the cooling process of a melt of a crystalline material, small crystals, or grains, start to form at many locations. As the melt cools each of the grains grows by incorporating atoms from the liquid surroundings. In the area where two grains meet, called the grain boundary, the atoms are not ordered since the two grains do not generally have the same direction of their atomic planes.

If all grains have the same chemical composition, the metal is said to have one phase. More on metal structures can be found in textbooks in material science, for example [1].

5 Summary of Paper A

Supposedly identical components made of metal often show substantial differences in fatigue lives. The differences are apparent even during controlled tests with identical stress levels. One source of variation could be differences in the structure of the metal. The idea in Paper A is to use a simulated grain structure and apply the existing theory of crack propagation to study the influence of grain structure on fatigue life. A short crack growth model is used since the main part of the fatigue life occurs during the crack initiation phase.

The crack growth model is adapted from Navarro-de los Rios model for short crack growth under uniaxial loading [6]. The crack is modelled on the surface of the metal and consequently the three-dimensional structure is disregarded. Since the point here is to use a grain structure with grains of different sizes, the Navarro-de los Rios model, which is described for grains of equal size, has to be modified to the current situation.

In the simulations the metal grain structure is a Voronoi tessellation in two dimensions of points generated from a Poisson process. The crack path was determined and the crack was allowed to grow to a maximum, it could stop before, length ten times the mean grain size. The crack growth rate as a function of crack length and the number of cycles to failure were calculated, the latter resulting in a Wöhler curve for the short crack growth. Compared with the fatigue life of a metal with all grains equal in size, that is the original Navarro-de los Rios model, the fatigue lives in the simulations were shorter. The fatigue life decreased with increasing number of grains, probably reflecting the fact that with increasing number of grains there is a greater probability of finding a large grain, where the crack is assumed to start. The standard deviation of the logarithm of the life lengths conditional on finite life is in the order of 0.2-0.4.

As expected, grain size variation gives rise to shortened fatigue life and also fatigue life dependent on component size. However, only a part of the observed fatigue life variation is explained by the varying grain size according to the simulations.

6 Summary of Paper B

We consider two models of non-overlapping convex grains, which are generalisations of Matérn's two hard-core processes, see [4]. These models were described in [3] and are constructed as follows. Convex sets, called grains, are placed at points of a homogeneous Poisson process and the process is thinned by two different procedures. The first thinning scheme, called pairwise, gives independent weights to both points in a pair with overlapping grains and the point with strictly higher weight wins. New weights are assigned in every comparison. A point is kept only if it wins in all pairwise comparisons. The second scheme, called global, gives each point a weight once and for all, and the point with strictly higher weight is kept when comparing with weights of overlapping grains. The weight may depend on the size of the grain in both cases.

The second-order product densities, defined in Section 2, of the above models are derived when the grains have equal orientation. In the derivation the product densities, the thinning procedure can be thought of as a process giving marks to the original Poisson process. A point gets mark 0 if it is removed and mark 1 if it is retained. The second-order product density can then be written in terms of the intensity, λ, of the Poisson process and the two-point mark distribution $\mathcal{M}_{x_1,x_2}$ as

$$\varrho_{th}^{(2)}(x_1, x_2) = \mathcal{M}_{x_1,x_2}(m_1 = 1, m_2 = 1). \tag{2}$$

The two-point mark distribution is the distribution of the marks in x_1 and x_2 under the condition that there are points in x_1 and x_2. The main idea, when calculating the product density, is then to find the probability that two points in x_1 and x_2 both have marks 1. It is equal to the probability that no points of the original point process win over them. The number of points that win over x_1 or x_2 is Poisson distributed and the essential step, when deriving the product density, is to calculate the expectation of this distribution.

As spheres are an important special case, the product densities for the models are stated both for spheres of equal radii in Theorems 2 and 3 and for spheres having a certain radius distribution in Theorems 4 and 5. When the grains are convex sets with the same orientation, the product densities are stated in Theorems 6 and 7. Except for some special cases, the product densities must be calculated by means of a numerical integration.

In the case of spheres of equal size the pair-correlation, which is the product density divided by the squared intensity, is compared to a Poisson process with the same intensity, see Figure 3 below and also Figure 5 in Paper B. The comparisons is made in terms of the frequency of pairs of points with certain interpoint distances. For short distances, less than two

times the radius, the pair-correlation is 0, meaning that two points cannot exist at that distance. For a slightly larger distance, between two times and four times the radius, pairs of points occur more frequently than in a Poisson process. For even larger distances, larger than four times the radius, the frequency of point pairs is the same as in a Poisson process. As the intensity of the original Poisson process tends to infinity the frequency of point pairs, at a distance between two and four times the radius, in the global model gets smaller, but is still slightly larger than for a Poisson process. In the pairwise model on the other hand the frequency of pairs of point at this distance tends to infinity as the intensity of the original Poisson process tends to infinity.

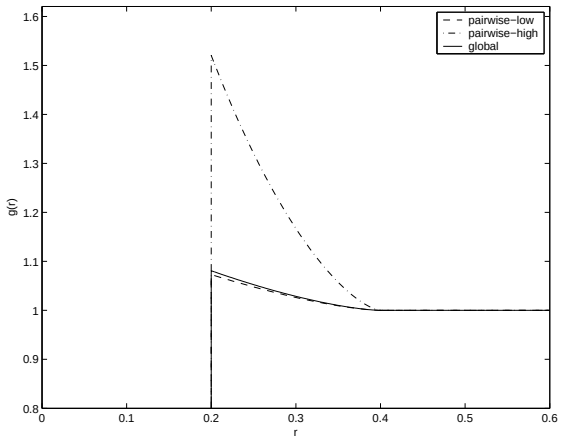

Figure 3: Pair-correlation function for the pairwise and the global model in two dimensions with the same intensity after thinning, $\lambda_{th} = 4$, and radius of the spheres $r_0 = 0.1$. The intensity before thinning was 5.74 and 34.11 for the two pairwise models giving the same λ_{th}, labelled low and high respectively in the plot, and 5.56 for the global.

By varying the size distribution and the weight distribution a wider range of behaviours of the product density can be obtained. This can, for example, be used in a future fitting to data of inclusions in steel.

7 Conclusions and future work

Common for both papers appended to the thesis is that we have used models from stochastic geometry to describe materials. The modelling is quite different in that the properties of the materials are modelled on two

different scales which shows the flexibility of this approach. However, the results are purely theoretical and have not yet been applied to the problems from which they originate.

In the future, the ideas from Paper A could be applied to a material for which there is real life data available. Then we could compare the variance in the theoretical results to the variance of the data and draw conclusions about the importance of the variability of grain sizes. Since the large grains in a grain structure seem to be of importance it would also be interesting to find the extreme value distribution of the largest grain in a Voronoi tessellation and also compare to real data.

The models in Paper B were inspired by images of inclusions in cast iron, see Figure 1, but it remains to be verified if they capture the features of these images. This could be done by estimating the product density from the images and compare them to the product densities of the models. The product densities of the models can be changed, to resemble the estimated product density, by introducing different radius distributions and different weight distributions.

References

[1] Callister Jr, W.D. (1997), *Materials, Science and Engineering : An Introduction*. Wiley.

[2] Hermann, H. (1991), *Stochastic Models of Heterogeneous Materials*. Material Science Forum, Vol. 78. Trans Tech Publications.

[3] Månsson, M., Rudemo, M. (2002), *Random patterns of nonoverlapping convex grains*. Adv. Appl. Prob. 34, 718-738.

[4] Matérn, B. (1960), *Spatial Variation*. Meddelanden Statens Skogsforskningsinst. 49. Statens Skogsforskningsinstitut, Stockholm, Second edition: Springer, Berlin, 1986.

[5] Möller, J. (1994), *Lecture Notes on Random Voronoi Tessellations*. Springer-Verlag.

[6] Navarro, A., de los Rios, E.R. (1988), *A microstructurally-short fatigue crack growth equation*. Fatigue Fract. Eng. Mater. Struct. Vol. 11, pp 383-396.

[7] Okabe, A., Boots, B., Sugihara, K. (1992), *Spatial Tessellations: Concepts and Applications of Voronoi Diagrams*. Wiley, 1992.

[8] Stoyan, D., Kendall, S.K., Mecke, J. (1995), *Stochastic Geometry and its Applications*. 2nd edition. Wiley.

Paper A

The influence of grain size variation on metal fatigue.

Jenny Andersson
Department of Mathematical Statistics, Chalmers University of Technology,
SE-412 96 Göteborg Sweden

Abstract

The aim of the present study is to investigate the influence of the variation of metal grain sizes on fatigue lives. The grain structure is simulated from a Poisson Voronoi model and the short crack growth model of Navarro and de los Rios is applied. The resulting fatigue life decreased with increasing component size, probably reflecting the fact that with increasing number of grains there is a larger probability of finding a large grain were the crack starts. The standard deviation of the logarithm of the lives was in the order of 0.2–0.4, i.e. the variation in grain size explains only part of the observed variance in real fatigue data.

Keywords: Short crack; Grain structure; Voronoi tessellation.

1 Introduction

Supposedly identical components made of metal often show substantial differences in fatigue lives. The differences are apparent even during controlled tests with identical stress levels. K. Miller writes in [1] that the scatter in fatigue data needs to be put in a perspective by for example detailed studies of the effect of material structure on early crack growth. One model of early (short) crack growth have been developed by A. Navarro and E.R. de los Rios in [3], [4], [5], [6], [7] and [8]. The purpose of this study is to investigate the effect of grain size variation on fatigue life. Since the main part of the fatigue life is explained by the crack initiation, the model of Navarro–de los Rios will be used, as in Turnbull and de los Rios [10], but modified to handle grains of varying sizes. A grain structure will be obtained by simulation. The grain model is introduced in section 2.1 and the Navarro–de los Rios model with modifications is described in section 2.2 along with some computational details. The results are presented in section 3 and analysed in section 4.

2 Model

2.1 Grain structure

In the proposed model the metal grain structure is a Voronoi tessellation in two or three dimensions of points generated from a Poisson process (see Figure 1). The reason for using a Voronoi tessellation can be argued as follows. If, in the crystallisation process of a one phase metal, all grains begin to grow simultaneously and at the same rate the resulting grain structure would be a Voronoi tessellation. The tessellation could be modified by allowing the grains to begin their growth at different times and by using a different point process with more or less clustering of the points.

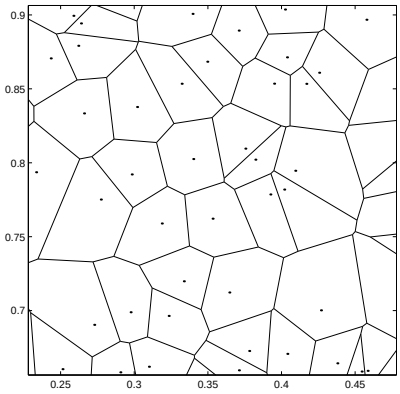

Figure 1: A Voronoi tessellation of points generated from a Poisson process

A tessellation partitions an Euclidean space ($\mathbb{R}^n$) into sets, (C_i), with non-overlapping interior, that is $\mathbb{R}^n = \cup_i C_i$. Let $\{p_i\}$ be a set of points. Each point p_i in this set, from now on called nuclei, generates a cell (or grain) C_i. One grain C_i consists of all points in $\mathbb{R}^n$ which has p_i as their nearest nuclei,

$$C_i = \{x \in \mathbb{R}^n : \|p_i - x\| \leq \|p_j - x\| \ , \forall p_j\}, \tag{1}$$

where $\|\cdot\|$ is the Euclidean distance. If the set of points $\{p_i\}$ is locally finite (any finite region contains a finite number of points) the C_i's are called a Voronoi tessellation and C_i a Voronoi cell. A general reference on the properties of Voronoi tessellations is [9] and a more mathematical one is [2].

The metal simulated here is assumed to have a face-centred cubic (FCC) atomic structure and one phase (homogeneous in terms of chemical composition).In the model each grain is given a random (uniformly distributed) slip plane direction which determines the directions for the other slip planes (Figure 2).

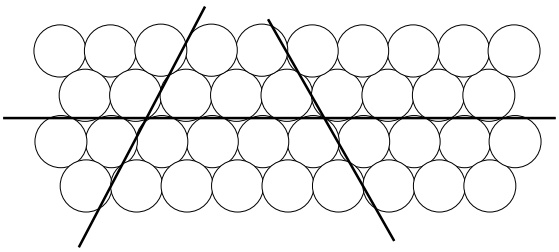

Figure 2: Slip planes in a closed packed metal seen in two dimensions.

2.2 Crack growth model

The crack growth model is adapted from Navarro-de los Rios model for short crack growth under uniaxial loading (references [3], [4], [5], [6], [7] and [8]). The crack is modelled on the surface of the metal and consequently the three dimensional structure is disregarded. Since the point here is to use a grain structure with grains of different sizes, the Navarro-de los Rios model, which is described for grains of equal size (as in Turnbull and de los Rios [10]), has to be modified to the current situation. In short the Navarro-de los Rios model considers the plastic slip produced ahead of a crack to be represented by a continuous distribution of dislocations. It is assumed that when slip is initiated in a grain the entire grain undergoes slip and is only blocked by the grain boundary, i.e. the front of the plastic zone coincides with the grain boundary. Slip is initiated in the next grain when the stress ahead of the plastic zone is enough to move new dislocations. This stress only depends on the position of the crack tip relative to the grain boundary.

The crack is initiated in the centre of a large grain with a slip plane close to the plane of maximum shear stress, that is the angle between the slip plane and the load direction is close to 45^o. In making a decision in which grain to start a compromise is made between size and direction of slip planes. If l is the length of the grain along a slip plain going through the centre of the grain and θ is the angle between the slip plane and the

plane of maximum shear stress, a new length is calculated by $l_c = l \cos 2\theta$ (this is repeated for the three slip planes through the centre of the grain). This calculation reflects the fact that the sheer is zero both perpendicular and parallel to the main load direction. The grain selected for the crack to start in is the one with maximal l_c. The crack is supposed to grow along a slip plane at all times.

The crack growth rate is determined by

$$\frac{da}{dN} = f\phi, \tag{2}$$

where a is half the surface crack length, N the number of load cycles, f represents the fraction of dislocations ahead of the crack that participates in the crack growth process and depends on the applied stress and the material and ϕ is the plastic displacement of the crack-tip given by

$$\phi = \frac{2(1-\nu)\sqrt{1-n^2}}{\mu n}\sigma a, \tag{3}$$

where σ is the applied load, μ the shear modulus and ν Poisson's ratio. Here $n = a/c$ is a dimensionless parameter, c the length of half the crack and half the plastic zone (see Figure 3).

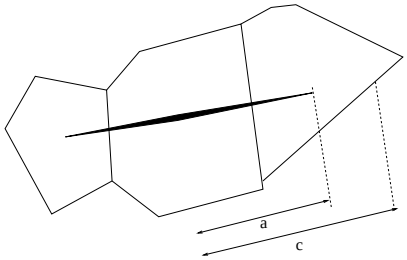

Figure 3: Illustration of the parameters c and a .

The slip band is blocked by the grain boundary and the crack will grow at a decreasing rate as it approaches the boundary until slip can be transfered to the next grain. This happens at a critical value of n equal to

$$n_c^i = \cos\left(\frac{\pi}{2}\frac{\sigma - \sigma_{Li}}{\sigma_{comp}}\right), \tag{4}$$

where σ_{comp} is the resistance to plastic deformation of the crack tip. Consecutive grains are numbered $i = 1, 2, 3, \ldots$. When σ is smaller than

σ_{Li} the stress is not enough to overcome the boundary and the crack stops. The minimum stress required for slip propagation is given by

$$\sigma_{Li} = \sigma_{FL} \frac{m_i}{m_1} \sqrt{\frac{\bar{d}_i}{2c_i}} \tag{5}$$

where c_i is the length of half the crack plus half the plastic zone when the crack grows in grain i, $\bar{d}_i$ is the mean of the length the crack has grown in each grain, σ_{FL} is the fatigue stress and

$$\frac{m_i}{m_1} = 1 + 2.07 \left(\frac{2}{\pi} \arctan\left(0.522(i-1)2\right) \right)^{1.86}. \tag{6}$$

is the ratio of grain orientations.

When a new slip band is initiated in the next grain and the plastic zone is supposed to span the entire new grain and therefore n decreases to

$$n_s^{i+1} = \frac{c_i}{c_{i+1}} n_c^i, \tag{7}$$

which is a rescaling of the old value of n by the new value of c. According to the model the crack will grow along that slip plane in the new grain that is closest to the plane of maximum shear stress (the angle between this plane and the loading direction is 45^o), regardless of which direction the slip plane takes in the third dimension under the surface.

The growth rate equation (2) can be integrated over a grain (or over parts of a grain) to give the number of cycles spent in that grain,

$$\Delta N_i = \frac{\mu}{f(1-\nu)2\sigma} \left(\arcsin n_c^i - \arcsin n_s^i \right). \tag{8}$$

The total number of cycles is then obtained by summing over all grains.

In the Navarro–de los Rios model all the grains are assumed to be equal in size and because of the symmetry in that case it is enough to do calculations on half the crack. Here however the crack may not grow at the same rate at both directions after the first grain. Practically this is solved by considering the two directions separately. For each direction (call them l = left and r = right respectively) it is possible to calculate a_r and a_l as functions of N. The total crack length as a function of N is $a_r + a_l$. The growth rate is calculated as $\phi(a_r) + \phi(a_l)$.

The values of the parameters used in the calculations are the same as Turnbull and de los Rios used in [10] for commercially pure Aluminium. These are shown in Table 1. They used $f = 6.16 \cdot 10^{-5}(2(\sigma - \sigma_{FL}))^{2.696}$.

Parameter	Value
μ	25.0 GPa
σ_{comp}	50.0 MPa
σ_{FL}	42.5 MPa
ν	0.33

Table 1: Parameter values for commercially pure Aluminium.

3 Results

Simulations were made of 2–dimensional Voronoi tessellations were the number of nuclei were taken from a Poisson distribution with expectation (denoted $A\lambda$) 2000, 4000 and 9000. The crack path was determined as described in section 2.2 and the crack was allowed to grow to a maximum (it could stop before, if $\sigma < \sigma_{Li}$ in equation (4)) length of ten times the mean grain size. The crack growth rate as a function of crack length and the number of cycles to failure were calculated, the latter resulting in a Wöhler curve for the short crack growth. For each value of the expectation the simulation was repeated 1000 times.

Figure 4 shows an example of a simulated crack and Figure 5 the crack growth rate as a function of crack length for this crack. In the latter figure there is also the corresponding plot for a grain structure with equal grain sizes. The growth rate decreases when the crack get close to a boundary, then increases sharply as the crack resumes its growth in the next grain. Figure 6 shows a Wöhler curve for the initial crack growth for expectation in the Poisson distribution equal to 9000. As a comparison the results from using a model without grain size variation is plotted in the same figure. A regression was made on the lives for $\Delta\sigma$ ranging from 94 MPa to 100 MPa to $N = a(\Delta\sigma)^b$ with the values of the coefficients in Table 2 as the result, i.e. the life decreases with $A\lambda$ or equivalently component size.

The observations at $N = 10^8$ are of cracks that have stopped before they were ten times the mean grain size long. The variation conditional on finite fatigue life of the number of cycles to failure first increases with the applied load and the decreases (plot in Figure 7). Figure 8 shows the percentage of cracks that stopped, i.e. the fatigue life is infinite.

Expectation ($A\lambda$)	$a \cdot 10^{44}$	b
1000	1.91	-23.7
4000	1.75	-23.7
9000	1.24	-23.6

Table 2: Coefficients in $N = a(\Delta\sigma)^b$.

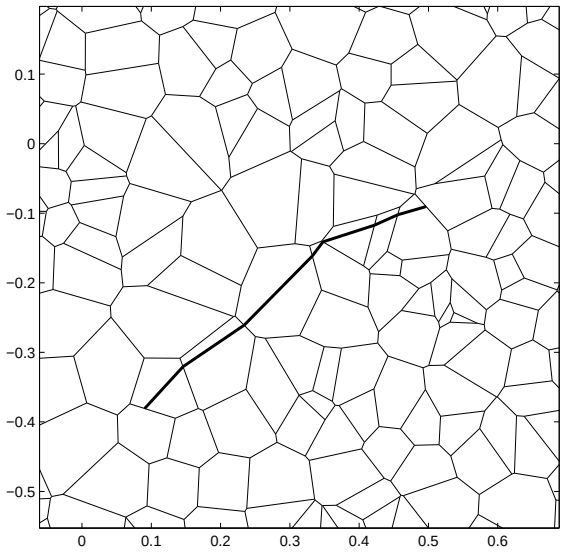

Figure 4: A simulated crack and grain structure

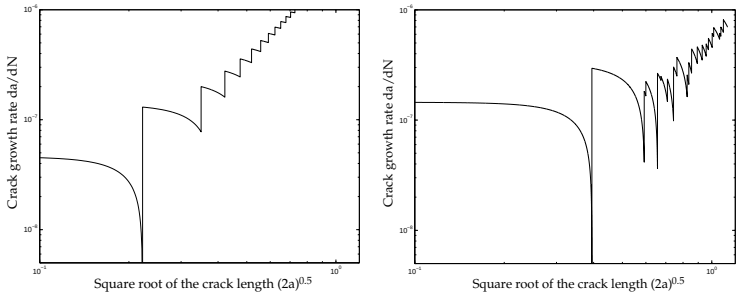

(a) Equal grains (b) Grain distribution

Figure 5: Logarithmic Crack growth rate plots for the original Navarro-de los Rios model to the left and for the Voronoi tessellation model to the right.

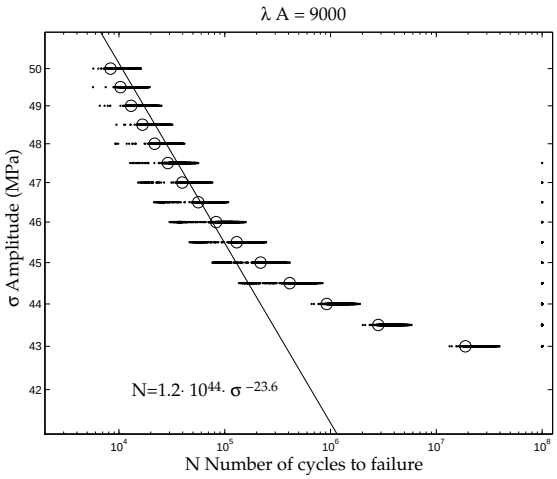

Figure 6: Wöhler curve for the initial crack growth. The unfilled rings corresponds to life lengths calculated from the model with equal grain sizes.

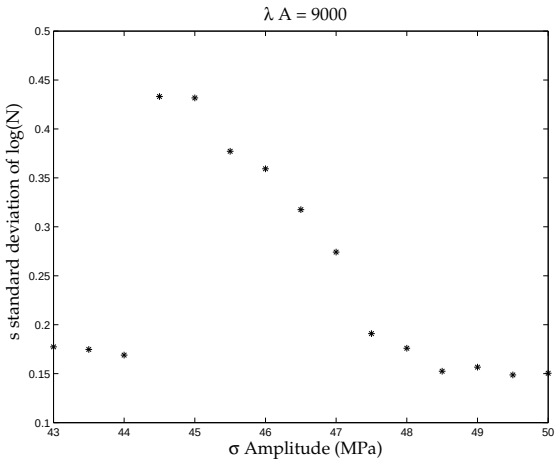

Figure 7: The standard deviation conditional on finite fatigue life of the number of cycles in Figure 6 as a function of the load.

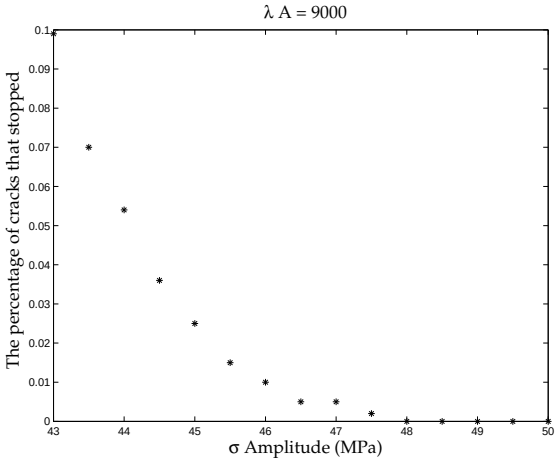

Figure 8: The percentage of cracks that stopped in Figure 6, i.e. the number of observations at $N = 10^8$ cycles.

4 Discussion

The discussion following is purely qualitative because of lack of real data. There is no evaluation of the Voronoi model as a grain structure and the calculated lives should be seen as an example of what is possible to do with this modelling approach. The crack growth model of Navarro–de los Rios is used only in the form of grains of equal sizes as a first approximation. For future simulations the results for unequal grain sizes in Vallellano, Navarro and Domínguez [11] can be used instead.

Comparing the simulations to a computation with equal grain sizes show that the crack growth rate curve is more irregular. The advantage of using a grain structure with varying grain sizes as opposed to one with equal grains is that the crack can stop and that it is possible to calculate the variance of the fatigue lives.

There are many simulations with infinite life even for higher loads which is not observed in real data. The explanation is that if a crack stops in a real material there may be a crack that can continue somewhere else in the structure. If a crack stops here there is no other crack that starts at another location. In principle it is possible to simulate that situation, however then a decision have to be made when to stop creating new cracks.

The standard deviation of the lives conditional on finite life first increases with the load and then decreases as expected from observations. The increase in the beginning is due to the censored data which really have large fatigue lives and hence would increase the standard deviation if they were accounted for.

The fatigue life decreased with increasing number of grains, probably reflecting the fact that with increasing number of grains there is a larger probability of finding a large grain (where the crack is assumed to start). The standard deviation of the logarithm of the lives conditional on finite life is in the order of 0.2–0.4 depending on the load.

As expected, grain size variation gives rise to shortened fatigue life and also fatigue life dependent on component size. However only a part of the observed fatigue life variation is explained by the varying grain size according to the simulations.

5 Acknowledgements

I am grateful to my supervisors Jacques de Maré and Thomas Svensson for starting me on this project and helpful discussions.

References

[1] Miller, K.J. A historical perspective of the important parameters of metal fatigue; and problems for the next century. Fatigue '99: Proc. 7th International Fatigue Congress, vols 1-4 , editors: X.R. Wu and Z.G. Wang, China Higher Education Press, Beijing, 1999, pp 15-39.

[2] Möller, J. Lecture notes on random Voronoi tessellations. Springer-Verlag, 1994.

[3] Navarro, A., de los Rios, E.R. A model for short fatigue crack propagation with an interpretation of the short-long transition. Fatigue Fract. Engng Mater. Struct. 1987:10:169-186.

[4] Navarro, A., de los Rios, E.R. A microstructurally-short fatigue crack growth equation. Fatigue Fract. Engng Mater. Struct. 1988:11:383-396.

[5] Navarro, A., de los Rios, E.R. Short and long fatigue crack growth: A unified model. Philosophical Magazine A 1988:57:15-36.

[6] Navarro, A., de los Rios, E.R. An alternative model of the blocking of dislocations at grain boundaries. Philosophical Magazine A 1988:57:37-42.

[7] Navarro, A., de los Rios, E.R. Compact solution for a multizone BCS crack model with bounded or unbounded end conditions. Philosophical Magazine A 1988:57:43-50.

[8] Navarro, A., de los Rios, E.R. Considerations of grain orientation and work hardening on short-fatigue-crack modelling. Philosophical Magazine A 1990:61:435-449.

[9] Okabe, A., Boots, B., Sugihara, K. Spatial tessellations: Concepts and applications of Voronoi diagrams. Wiley, 1992.

[10] Turnbull, A., de los Rios, E. R. Predicting fatigue life in commercially pure aluminium using a short crack growth model. Fatigue Fract. Engng Mater. Struct. 1995:18:1469-1481.

[11] Vallellano C., Navarro A., Domínguez J., Compact formulation for modelling cracks in infinite solids using distributed dislocations. Philosophical Magazine A 2002:82:81-92.

Paper B

Product densities of two models of non-overlapping grains

Jenny Andersson

9th December 2003

Abstract

We consider two models of non-overlapping convex grains, which are generalisations of Matérn's two hard-core processes. Grains are placed at points of a homogeneous Poisson process and the process is thinned by two different procedures. The second-order product density is derived for the point process with convex grains of equal orientation. As spheres are an important special case, the product densities for the models are stated both for spheres of equal radii and for spheres having a certain radius distribution.

1 Introduction

A point process where the points cannot be closer than a fixed minimal distance is called a hard-core point process. Matérn [4] introduced two such processes. In the first one he considers a Poisson process and excludes every point with a distance to its nearest neighbour less than a fixed number $R > 0$. In the second model each point is given a weight, uniformly distributed on $(0, 1)$ and independent of the weights of other points. Points are then retained if there are no other points within distance R with lower weight and removed otherwise. These models can be thought of as systems of non-overlapping spheres with radii $R/2$. A survey of random systems of non-intersecting spheres is found in [9]. Hard-core models are used, for example in forestry applications, see [11].

Another example of hard-core models is the simple sequential inhibition model, SSI, which is also called the random sequential adsorption model, RSA, used in physical and biological sciences. Spheres are placed randomly and sequentially in a bounded region. A sphere is rejected if it intersects a previously placed sphere. Other items than spheres could be used. For a survey on RSA models, see for example [14].

The Stienen model and a generalisation, the lily-pond model, describe sets of spheres with random radii. Points are generated according to a stationary Poisson process. In the Stienen model, each Poisson point is the centre of a sphere with a diameter equal to the distance to its nearest neighbour. See [8] and pages 218 and 380 in [10] for more on the Stienen model, for example the pair-correlation function. In the lily-pond model spheres are grown radially, at the same time and at the same rate, from the Poisson points. Each sphere grows until it meets another sphere. In [1] there are some recent results and an overview of what is known so far for the lily-pond model.

Some hard-core models are examples of Gibbs processes, which are also studied in the literature on physics. A mathematical treatment can be found in [10].

A model which is closely related to Matérn's second model is Matheron's dead leaves model, see [2] and [12]. In two dimensions, discs are dropped sequentially according to a Poisson process on the plane. Parts of a new disc that intersects an old disc are invisible, that is we watch the discs from below. In a finite area, the process can be stopped once all the surface is covered by discs, since new discs dropped do not influence the distribution of the intact discs. The intact discs correspond to the points that are not removed in Matérns second model when the intensity of the Poisson process tends to infinity, according to [12].

Månsson and Rudemo [3] describe two models of non-overlapping grains, which are generalisatations of Matérns models. The processes are obtained by thinning a stationary Poisson process. A convex compact set, called grain, is associated with each point. In the simplest case the grains are spheres with equal radii. Points with overlapping grains are either removed or kept, according to two different procedures, in a way that leaves points with non-overlapping grains. The first thinning scheme, called pairwise, gives independent weights to both points in a pair with overlapping grains, and the point with strictly higher weight wins. New weights are assigned in every comparison. A point is kept only if it wins in all pairwise comparisons. The second scheme, called global, gives each point a weight once and for all and the point with strictly higher weight is kept when comparing with weights of overlapping grains. The weight may depend on the size of the grain in both cases. Figure 1 is a realisation of these models for spheres of equal sizes. The models in [3] were originally inspired by inclusions in steel and nodular cast iron, which are important for the fatigue strength of these materials.

Similar to the models in [3] are the generalisations of Matérn's second model in [13]. In the first generalisation the weights may have some distribution that is not uniform and which is independent of the radius. As in

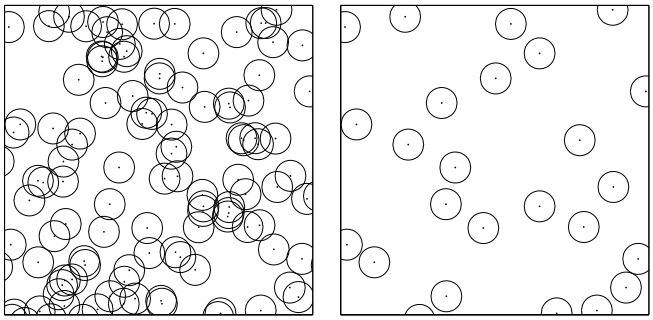

(a) Before thinning

(b) Pairwise thinning

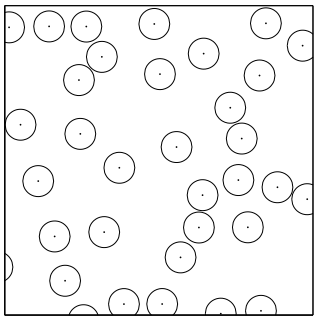

(c) Global thinning

Figure 1: Realisation of pairwise and global thinning of a Poisson process in the unit square of $\mathbb{R}^2$ with intensity $\lambda = 100$, where all the spheres have an equal radius 0.05.

Matérn's model, a point in x is removed if there is another point in the ball of radius R, centred in x with lower weight than x. This gives exactly the same point process after thinning as in the global model above with the same weight distribution and all radii equal to $R/2$. In the second generalisation, the radii of the points are not constant but follow some distribution, that is a point x gets radius r_x. A point in x is now removed if there is no other point with lower weight in the sphere with radius r_x centred at x.

This is not a model of non-overlapping spheres as the global model of [3]. For example, it is possible to have one sphere completely inside another. In [13] thinning intensities and product-densities for both models are derived.

In [3], the thinning probabilities, the relation between the point processes before and after thinning, the volume fraction and the size distributions after thinning are considered. To further characterise these models we are interested in studying second-order characteristics. Once a second-order measure and the first moment measure are known, variances and covariances can be calculated. Furthermore, the second-order properties can be used to compare the models, for example to a stationary Poisson process.

We start by giving a description of the pairwise and global models in Section 2. We define the product density and derive an expression for calculating the product density in terms of a two-point mark probability in Section 3. This expression is used in [6] and [7]. In Section 4 we calculate the second-order product density for spherical grains with fixed radii for the two thinning procedures. This may seem somewhat superfluous as the same calculations for general radius distribution are carried out in Section 5, but we think it is worthwhile to present the ideas of the proofs in an easier setting. Section 6 states the product densities for convex, compact grains with the same orientation.

2 Description of the models

Consider a Poisson point process with constant intensity λ in $\mathbb{R}^d$. On each point a sphere, or some other convex set, in general called grain, is centred. The radius of the sphere associated with a point has distribution F_R, which is independent of the point process and of the radii of other points. The process is thinned so that there are no intersecting spheres, according to two different schemes:

(P) Pairwise assignment of weights. For each pair of points with intersecting spheres both points get weights independent of each other and the point with the lower weight is removed. In the case of equal weights both are removed. A point will only be retained if it wins in each of the pairwise comparisons. For example, if three points have intersecting spheres it is possible that all three points will be removed.

(G) Global assignment of weights. The points get i.i.d. weights once and for all. As before, points with intersecting spheres compete and the one with strictly higher weight is retained.

Both in the global and pairwise case the weight may depend on the radius, but not on the point process. Denote the weight distribution for a sphere with radius r by $F_{W|r}$.

The thinning procedure can be thought of as giving marks to the original Poisson process. A point gets mark 1 if it is kept and 0 if it is removed. Now we have a marked process $\Phi = \{[X_n; M_n]\}$ with points $\{X_n\}$ constituting a stationary Poisson process with intensity λ in $\mathbb{R}^d$ and to each X_n an associated mark M_n taking values in $M = \{0, 1\}$.

The intensity is an important characteristic of a point process. For the current models it can be expressed in terms of $h(r)$, the retaining probability, i.e. the probability that a point with radius r will be retained (see [3]), as

$$\lambda_{th} = \lambda \int_0^\infty h(r) F_R(\mathrm{d}r). \tag{1}$$

Let $W_1(r)$ and $W_2(y)$ be two independent weights with distribution functions $F_{W|r}$ and $F_{W|y}$, and κ_d the volume of the unit sphere in d dimensions. The retaining probability for the pairwise case is

$$h_P(r) = \exp\left\{-\lambda\kappa_d \int_0^\infty \mathbb{P}(W_1(r) \le W_2(y))(r+y)^d F_R(\mathrm{d}y)\right\}. \tag{2}$$

For the global case the retaining probability is

$$h_G(r) = \int_0^\infty \exp\left\{-\lambda\kappa_d \int_0^\infty (1 - F_{W|y}(w))(r+y)^d F_R(\mathrm{d}y)\right\} F_{W|r}(\mathrm{d}w). \tag{3}$$

A further characteristic of these models is the radius distribution after thinning. In general it is not the same as the distribution before thinning, but the right tail of the distribution can be preserved, if large spheres are kept in the thinning. See [3] for a discussion of the radius distribution.

3 Second-order quantities

As mentioned in the Introduction, we want to study functions that describe the second-order behaviour of these models. One such function is the second-order product density $\varrho^{(2)}$. It is the density with respect to the Lebesgue measure of the second-order factorial moment measure $\alpha^{(2)}$ on $\mathbb{R}^d \times \mathbb{R}^d$. If B_1 and B_2 are Borel sets and Ψ is a point process on $\mathbb{R}^d$ with distribution P_Ψ, $\alpha^{(2)}$ is defined as

$$\begin{aligned}\alpha^{(2)}(B_1 \times B_2) =& \mathbb{E}[\#\{(x,y) : x \in \Psi \cap B_1, y \in \Psi \cap B_2, x \neq y\}] \\ =& \int \sum_{\substack{x_1, x_2 \in \psi \\ x_1 \neq x_2}} 1_{B_1}(x_1) 1_{B_2}(x_2) P_\Psi(\mathrm{d}\psi).\end{aligned}$$

An interpretation of the second-order product density is that

$$\varrho^{(2)}(x,y)dV_1dV_2$$

is the probability of having a point in each of two infinitesimally small disjoint Borel sets, with Lebesgue measures dV_1 and dV_2, where x and y belong to one set each. The following result will be used in the calculation of the second-order product density for the thinned processes defined above.

Lemma 1 *Let $\Phi = \{[X_n; M_n]\}$ be a simple marked point process in $\mathbb{R}^d$ with marks in $M = \{0,1\}$, where the associated point process $\{X_n\}$ is a stationary Poisson process with intensity λ and $\mathcal{M}_{x_1,x_2}$ is the two-point mark distribution, defined on $M \times M$. Then the second-order product density $\varrho_{th}^{(2)}$ for the process consisting of points with marks 1 can be written as*

$$\varrho_{th}^{(2)}(x_1,x_2) = \lambda^2 \mathcal{M}_{x_1,x_2}(m_1 = 1, m_2 = 1). \tag{4}$$

If the process consisting of points with marks 1 is stationary and isotropic the product density will only depend on the distance $|x_1 - x_2|$ between the two points, and $\varrho_{th}^{(2)}(x_1,x_2)$ is simplified to

$$\varrho_{th}^{(2)}(r) = \lambda^2 \mathcal{M}_{o,\boldsymbol{r}}(m_o = 1, m_{\boldsymbol{r}} = 1), \tag{5}$$

for one point at the origin and one point in location $\boldsymbol{r}$ at distance r from the origin.

The two-point mark distribution $\mathcal{M}_{x_1,x_2}$ describes the marks in x_1 and x_2 under the condition that there are points in x_1 and x_2, see [5]. It can be thought of as a two-fold Palm distribution.

The proof of Lemma 1, which is given below, is rather technical and may be skipped without affecting the reading of further sections. We need a modification of Theorem 2.3 from [5] with the assumption of the stationarity and isotropy of the marked process removed. The proof of this modification can essentially be found in [5], but is not stated in a theorem there. The theorem below, which states the modification, can be called the "two-point Campbell theorem".

Theorem 1 *Let $\Phi = \{[X_n; M_n]\}$ be a simple marked point process in $\mathbb{R}^d$ with marks in $M = \{0,1\}$ and distribution P. The set of all outcomes of Φ is denoted by N. Let $\{\mathcal{M}_{x_1,x_2} : x_1, x_2 \in \mathbb{R}^d\}$ be the family of corresponding two-point mark distributions and let $\alpha_{(2)}$ be the second-order factorial mo-*

ment measure of $\{X_n\}$. *For every measurable* $f : \mathbb{R}^d \times M \times \mathbb{R}^d \times M \to \mathbb{R}^+$,

$$\int_N \sum_{\substack{[x_1;m_1]\in\varphi \\ [x_2;m_2]\in\varphi \\ x_1\neq x_2}} f(x_1,m_1,x_2,m_2)P(\mathrm{d}\varphi)$$
$$= \int_{\mathbb{R}^d\times\mathbb{R}^d} \int_{M\times M} f(x_1,m_1,x_2,m_2)\mathcal{M}_{x_1,x_2}(\mathrm{d}(m_1,m_2))\alpha_{(2)}(\mathrm{d}(x_1,x_2)).$$

Now we are ready to prove Lemma 1 with the aid of Theorem 1.

Proof of Lemma 1 For a thinned process with distribution P_{th} the second-order factorial moment measure is

$$\alpha^{(2)}_{th}(B_1\times B_2) = \int \sum_{\substack{x_1\in\varphi,\ x_2\in\varphi \\ x_1\neq x_2}} 1_{B_1}(x_1)1_{B_2}(x_2)P_{th}(\mathrm{d}\varphi).$$

This expression can be rewritten in terms of the original marked process Φ with distribution P. Let $1_{\{1\}\times\{1\}}(m_1,m_2)$ be the indicator function of the event that both x_1 and x_2 are retained when thinning. By summing over all points in Φ that are retained in the thinning procedure we get

$$\alpha^{(2)}_{th}(B_1\times B_2) = \int_N \sum_{\substack{[x_1;m_1]\in\varphi \\ [x_2;m_2]\in\varphi \\ x_1\neq x_2}} 1_{B_1}(x_1)1_{B_2}(x_2)1_{\{1\}\times\{1\}}(m_1,m_2)P(\mathrm{d}\varphi).$$

By Theorem 1,

$$\alpha^{(2)}_{th}(B_1\times B_2)$$
$$= \int_{B_1\times B_2}\int_{M\times M} 1_{\{1\}\times\{1\}}(m_1,m_2)\mathcal{M}_{x_1,x_2}(\mathrm{d}(m_1,m_2))\alpha^{(2)}(\mathrm{d}(x_1,x_2))$$
$$= \int_{B_1\times B_2} \sum_{m_1=0}^{1}\sum_{m_2=0}^{1} 1_{\{1\}\times\{1\}}(m_1,m_2)\mathcal{M}_{x_1,x_2}(\mathrm{d}(m_1,m_2))\alpha^{(2)}(\mathrm{d}(x_1,x_2))$$
$$= \int_{B_1\times B_2} \mathcal{M}_{x_1,x_2}(\{1\}\times\{1\})\alpha^{(2)}(\mathrm{d}(x_1,x_2))$$
$$= \int_{B_1\times B_2} \mathcal{M}_{x_1,x_2}(m_1=1,m_2=1)\alpha^{(2)}(\mathrm{d}(x_1,x_2)).$$

For a homogeneous Poisson process with intensity λ, the second-order factorial moment measure $\alpha^{(2)}(B_1\times B_2) = \lambda^2 l_d(B_1)l_d(B_2)$, see for example

[10]. Since the product density of the thinned process is the density of $\alpha_{th}^{(2)}$ with respect to Lebesgue measure we get (4). □

4 Spheres with fixed radii

4.1 Second-order product densities

In this section we derive the second-order product density for the two point processes with spheres of radius r_0 and continuous weight distribution. The following notation is used. Let $B_d(x,r) = \{y \in \mathbb{R}^d : |x-y| \leq r\}$ be the d-dimensional sphere centred in x with radius r and let l_d be the Lebesgue measure in $\mathbb{R}^d$. Moreover, let $\kappa_d = l_d(B(x,1))$, the volume of the unit d-dimensional sphere, so that $l_d(B(x,r)) = \kappa_d r^d$, and let $\gamma_d(r,h) = l_d(B_d(x,h) \cap B_d(x+r,h)$ be the volume of the intersection of two spheres with equal radius h with centres at a distance r from each other, see Appendix A for calculations in two and three dimensions. Quantities in the pairwise case and the global case are indexed by P and G, respectively.

From equations (1), (2) and (3), the intensities of the thinned processes are

$$\lambda_{thP} = \lambda \ \exp\left\{-\frac{1}{2}\lambda\kappa_d(2r_0)^d\right\}$$

in the pairwise model and

$$\lambda_{thG} = \frac{1-\exp\left\{-\lambda\kappa_d(2r_0)^d\right\}}{\kappa_d(2r_0)^d},$$

in the global model, when the intensity of the Poisson process before thinning is λ.

Theorem 2 *With pairwise assignment of weights, the second-order product density is*

$$\varrho^{(2)}(r) = \begin{cases} 0 & \text{if } r \leq 2r_0 \\ \lambda^2 \exp\left\{-\lambda(\kappa_d(2r_0)^d - \frac{1}{4}\gamma_d(r,2r_0))\right\} & \text{if } 2r_0 < r \leq 4r_0 \\ \lambda^2 \exp\left\{-\lambda\kappa_d(2r_0)^d\right\} & \text{if } r > 4r_0. \end{cases} \quad (6)$$

Proof We use (5) to calculate the product density, i.e. we need $\mathcal{M}_{o,\boldsymbol{r}}(m_o = 1, m_{\boldsymbol{r}} = 1)$, the two-point mark probability that two points at distance r both have marks 1, that is the probability of retaining two points at distance r. Given one point at the origin, o, and one point at distance r from the origin located in $\boldsymbol{r}$, see Figure 2, the probability that both points

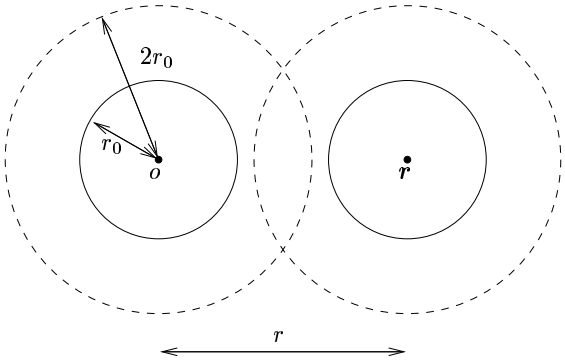

Figure 2: Two spheres at distance r in 2-d.

are retained is zero if $r \leq 2r_0$, since then their spheres intersect and at least one of them must be removed and hence $\mathcal{M}_{o,\boldsymbol{r}}(m_o = 1, m_{\boldsymbol{r}} = 1) = 0$. For $r > 2r_0$ the two-point mark probability can be rewritten as

$$\mathcal{M}_{o,\boldsymbol{r}}(m_o = 1, m_{\boldsymbol{r}} = 1) = \mathbb{P}(\{\#\text{ of points that win over } o \text{ or } \boldsymbol{r}\} = 0). \quad (7)$$

The points that win over o or $\boldsymbol{r}$ constitute an inhomogeneous Poisson process with intensity function $\lambda_b(x)$. When λ is the intensity of the Poisson process before thinning, the mean number of points in $\mathbb{R}^d$ of this inhomogeneous process can be written

$$\int_{\mathbb{R}^d} \lambda_b(x)\mathrm{d}x = \int_{\mathbb{R}^d} \lambda \mathbb{P}(\text{A point in } x \text{ wins over } o \text{ or } \boldsymbol{r})\mathrm{d}x.$$

For $r > 2r_0$ points that belongs to the union of $B_d(o, 2r_0)$ and $B_d(\boldsymbol{r}, 2r_0)$ are possible candidates for winning over either o or $\boldsymbol{r}$ or both. More precisely points in $B_d(o, 2r_0) \setminus B_d(\boldsymbol{r}, 2r_0)$ can beat o, but not $\boldsymbol{r}$, points in $B_d(\boldsymbol{r}, 2r_0) \setminus B_d(o, 2r_0)$ can beat $\boldsymbol{r}$, but not o and points in $B_d(o, 2r_0) \cap B_d(\boldsymbol{r}, 2r_0)$ can beat o or $\boldsymbol{r}$. If W_o is the weight of o, $W_{\boldsymbol{r}}$ is the weight of $\boldsymbol{r}$, W_{x1} is the weight of x when competing with o and W_{x2} is the weight of x when competing with $\boldsymbol{r}$, then

$$\begin{aligned}\int_{\mathbb{R}^d} \lambda_b(x)\mathrm{d}x =& \lambda \int_{\mathbb{R}^d} \Big[1_{\{B_d(o,2r_0)\setminus B_d(\boldsymbol{r},2r_0)\}}(x)\mathbb{P}(W_{x1} \geq W_o) \\ &+ 1_{\{B_d(\boldsymbol{r},2r_0)\setminus B_d(o,2r_0)\}}(x)\mathbb{P}(W_{x2} \geq W_{\boldsymbol{r}}) \\ &+ 1_{\{B_d(\boldsymbol{r},2r_0)\cap B_d(o,2r_0)\}}(x)\mathbb{P}(W_{x1} \geq W_o \cup W_{x2} \geq W_{\boldsymbol{r}})\Big]\mathrm{d}x \end{aligned} \quad (8)$$

since the sets are disjoint. Further simplification gives,

$$\begin{aligned}\int_{\mathbb{R}^d}\lambda_b(x)\mathrm{d}x &= \lambda\int_{\mathbb{R}^d}\Big[1_{\{B_d(o,2r_0)\setminus B_d(\boldsymbol{r},2r_0)\}}(x)\frac{1}{2}\\ &\quad + 1_{\{B_d(\boldsymbol{r},2r_0)\setminus B_d(o,2r_0)\}}(x)\frac{1}{2} + 1_{\{B_d(\boldsymbol{r},2r_0)\cap B_d(o,2r_0)\}}(x)\frac{3}{4}\Big]\mathrm{d}x\\ &= \lambda\Big[\frac{1}{2}l_d(B_d(o,2r_0)\setminus B_d(\boldsymbol{r},2r_0)) + \frac{1}{2}l_d(B_d(\boldsymbol{r},2r_0)\setminus B_d(o,2r_0))\\ &\quad + \frac{3}{4}l_d(B_d(\boldsymbol{r},2r_0)\cap B_d(o,2r_0))\Big].\end{aligned} \tag{9}$$

Recalling (7) we get

$$\mathcal{M}_{o,\boldsymbol{r}}(m_o = 1, m_{\boldsymbol{r}} = 1) = \exp\Big\{-\int_{\mathbb{R}^d}\lambda_b(x)\mathrm{d}x\Big\}. \tag{10}$$

Equations (9) and (10) combined with (5), using

$$\begin{aligned}&l_d(B_d(o,2r_0)\setminus B_d(\boldsymbol{r},2r_0)) = l_d(B_d(\boldsymbol{r},2r_0)\setminus B_d(o,2r_0))\\ &= \kappa_d(2r_0)^d - \gamma_d(r,2r_0)\end{aligned}$$

and

$$l_d(B_d(\boldsymbol{r},2r_0)\cap B_d(o,2r_0)) = \gamma_d(r,2r_0)$$

concludes the proof. Observe that $\gamma_d(r,2r_0) = 0$ for $r > 4r_0$. □

Theorem 3 *Let $V = \kappa_d(2r_0)^d$ and $q(r) = \gamma_d(r,2r_0)$. With global assignment of weights, the second-order product density is*

$$\varrho^{(2)}(r) = \begin{cases} 0 & \text{if } r \le 2r_0\\ 2\Big\{\dfrac{1}{V(2V-q(r))} - \dfrac{e^{-\lambda V}}{V(V-q(r))} & \\ \qquad + \dfrac{e^{-\lambda(2V-q(r))}}{(V-q(r))(2V-q(r))}\Big\} & \text{if } 2r_0 < r \le 4r_0\\ \left(\dfrac{1-e^{-\lambda V}}{V}\right)^2 & \text{if } r > 4r_0. \end{cases} \tag{11}$$

Remark: This formula can be found on page 164 in [10]. The proof given here is very similar to that of Theorem 2.

Proof Conditioning on the probability that a point in o has weight w_o and a point in $\boldsymbol{r}$, at distance r from the origin, has weight $w_{\boldsymbol{r}}$, the probability that both points are retained can be found as in the proof of Theorem 2

above. Denote a point in x having radius r_x by $[x; r_x]$. For simplicity's sake we take the weight distribution to be uniform, but it could be any continuous distribution. Instead of (7) we get

$$\mathcal{M}_{o,\boldsymbol{r}}(m_o = 1, m_{\boldsymbol{r}} = 1)$$
$$= \int_0^1 \int_0^1 \mathbb{P}(\{\#\text{ of points that win over } [o; w_o] \text{ or } [\boldsymbol{r}; w_{\boldsymbol{r}}]\} = 0) \mathrm{d}w_o \mathrm{d}w_{\boldsymbol{r}}.$$

Another difference from the proof of Theorem 2 is that in (8)

$$\mathbb{P}(W_{x1} \geq W_o) \text{ is replaced by } \mathbb{P}(W_x \geq w_o) = \int_{w_o}^1 \mathrm{d}w = 1 - w_o,$$
$$\mathbb{P}(W_{x2} \geq W_{\boldsymbol{r}}) \text{ is replaced by } \mathbb{P}(W_x \geq w_{\boldsymbol{r}}) = \int_{w_{\boldsymbol{r}}}^1 \mathrm{d}w = 1 - w_{\boldsymbol{r}}$$

and similarly

$$\mathbb{P}(W_{x1} \geq W_o \cup W_{x2} \geq W_{\boldsymbol{r}}) \text{ is replaced by}$$
$$\mathbb{P}(W_x \geq min(w_o, w_{\boldsymbol{r}})) = \int_{min(w_o, w_{\boldsymbol{r}})}^1 \mathrm{d}w = 1 - min(w_o, w_{\boldsymbol{r}}).$$

This leads to

$$\begin{aligned} &\mathcal{M}_{o,\boldsymbol{r}}(m_o = 1, m_{\boldsymbol{r}} = 1) \\ &\quad = \int_0^1 \int_0^1 \exp\Big\{ -\lambda\big[(1 - w_o)(\kappa_d(2r_0)^d - \gamma_d(r, 2r_0)) \\ &\qquad + (1 - w_{\boldsymbol{r}})(\kappa_d(2r_0)^d - \gamma_d(r, 2r_0)) \\ &\qquad + (1 - min(w_{\boldsymbol{r}}, w_o))\gamma_d(r, 2r_0)\big]\Big\} \mathrm{d}w_o \mathrm{d}w_{\boldsymbol{r}}. \end{aligned} \tag{12}$$

Evaluating (12) and multiplying by λ^2 gives (11). □

4.2 Behaviour of the models

According to [3] the intensities after thinning behave quite differently for the two models, see Figure 3. For the pairwise case $\lambda_{th} \to 0$ as $\lambda \to \infty$ and it has a maximum in $\lambda_{th} = 2/(\kappa_d(2r_0)^d e)$ for $\lambda = 2/(\kappa_d(2r_0)^d)$. On the other hand, for the global case, λ_{th} is increasing in λ and as $\lambda \to \infty$, $\lambda_{th} \to 1/(\kappa_d(2r_0)^d)$.

When comparing product densities of the global model and the pairwise model it is clearer to consider the pair-correlation function instead. It is defined as

$$g(r) = \varrho^{(2)}(r)/\lambda_{th}^2,$$

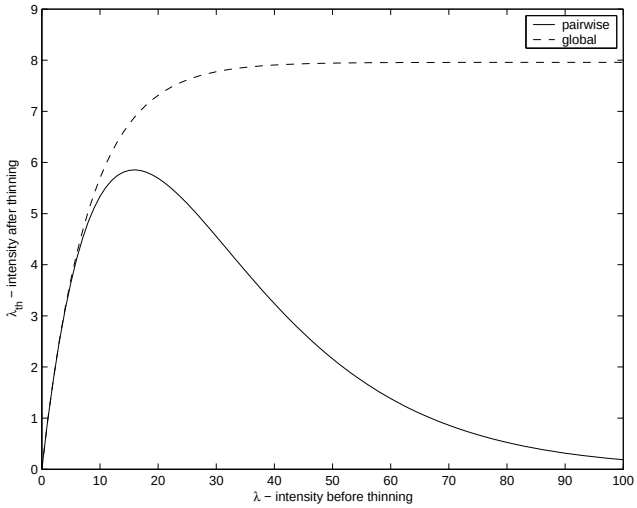

Figure 3: The intensity after thinning for the pairwise and the global models in two dimensions for spheres of equal radii=0.1.

giving

$$g_P(r) = \begin{cases} 0 & \text{if } r \leq 2r_0 \\ \exp\left\{\lambda \frac{1}{4}\gamma_d(r, 2r_0)\right\} & \text{if } 2r_0 < r \leq 4r_0 \\ 1 & \text{if } r > 4r_0 \end{cases}$$

and

$$g_G(r) = \begin{cases} 0 & \text{if } r \leq 2r_0 \\ \dfrac{2}{\lambda_{thG}^2}\left\{\dfrac{1}{V(2V - q(r))} - \dfrac{e^{-\lambda V}}{V(V - q(r))} + \dfrac{e^{-\lambda(2V - q(r))}}{(V - q(r))(2V - q(r))}\right\} & \text{if } 2r_0 < r \leq 4r_0 \\ 1 & \text{if } r > 4r_0, \end{cases}$$

for the two models. For a Poisson process $g(r) = 1$, $r > 0$, see [10]. When $r \leq 2r_0$, the pair-correlation is 0 and there can be no pair of points with such a distance between the points. The pair-correlation is 1 for both models when $r > 4r_0$, meaning that the frequency of point pairs at distances larger than $4r_0$ is the same as in a Poisson process. For the

pairwise model and $2r_0 < r \leq 4r_0$, the pair-correlation is increasing in λ, meaning that when $\lambda \to \infty$ the process has a higher frequency of pairs of points at distances between $2r_0$ and $4r_0$ than a homogeneous Poisson process even though the intensity after thinning tends to zero at the same time. On the other hand, when λ goes to infinity for the global model, g_G tends to $(2V)/(2V - q(r))$, for $2r_0 < r \leq 4r_0$, which is between 1 and 1.1 in $\mathbb{R}^2$, since $0 \leq q(r)/V < 2/3 - \sqrt{3}/\pi$. In $\mathbb{R}^d$ an upper bound for $q(2r_0)$ is $1/2$, meaning that $(2V)/(2V - q(r))$ is never greater than $4/3$. This means that the global process has almost the same pair-correlation as a Poisson process except for the hard cores. When $\lambda \to 0$ the two processes behave alike in that both $\lambda_{th} \to 0$ and $g(r) \to 1$, for $r > 2r_0$.

If we compare the pair-correlation functions for the same value of the intensity after thinning we get three different behaviours since the pairwise model can have the same λ_{th} for two different λ, as can be seen in Figure 3. Figure 4 and Figure 5 show a plot of the pairwise and the global pair-correlation function in two dimensions.

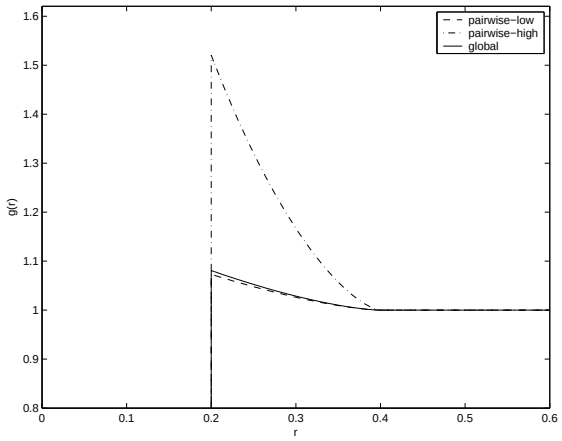

Figure 4: Pair-correlation function for the pairwise and the global model in two dimensions with the same intensity after thinning, $\lambda_{th} = 4$, and radius of the spheres $r_0 = 0.1$. The intensity before thinning was 5.74 and 34.11 for the two pairwise models giving the same λ_{th}, labelled low and high respectively in the plot, and 5.56 for the global.

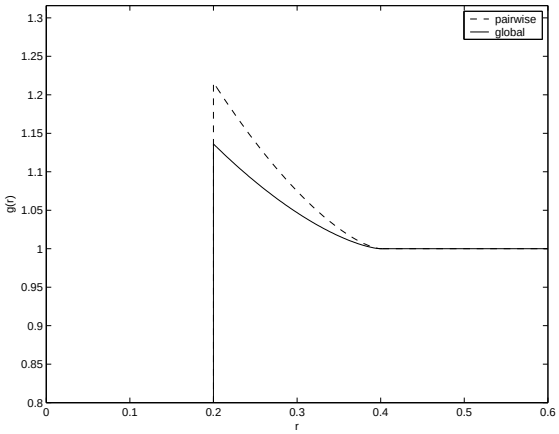

Figure 5: Pair-correlation function for the pairwise and the global model in two dimensions with the same intensity after thinning, $\lambda_{th} = 2/(\kappa_d(2r_0)^d e) = 5.86$, and radius of the spheres $r_0 = 0.1$. The intensity before thinning was 15.92 for the pairwise model and 10.59 for the global. Compared with Figure 4 there is only one pairwise model since λ_{th} is chosen as the maximum in Figure 3.

5 Spheres with general radius and weight distributions

Now we turn to a more general case than above, where the spheres radii have some nondegenerate distribution, as a step towards convex sets of varying sizes in Section 6. Let the spheres have radius distribution F_R and the weights have distribution $F_{W|r}$ which may depend on the radius.

Theorem 4 *Let* $\delta_d(r, r_o + r_w, r_{\boldsymbol{r}} + r_w) = l_d(B_d(o, r_o + r_w) \cap B_d(\boldsymbol{r}, r_{\boldsymbol{r}} + r_w))$ *with* $|o - \boldsymbol{r}| = r$ *and let* $W_i(x)$ *have distribution* $F_{W|x}$. *With pairwise assignment of weights, the second-order product density is*

$$\begin{aligned}\varrho^{(2)}(r) = \lambda^2 \int_0^r \int_0^{r-r_o} \exp\Big\{-\lambda \int_0^\infty \\ \Big[\big(\kappa_d(r_o + r_w)^d - \delta_d(r, r_o + r_w, r_{\boldsymbol{r}} + r_w)\big)\mathbb{P}(W_1(r_o) \le W_2(r_w)) \\ + \big(\kappa_d(r_{\boldsymbol{r}} + r_w)^d - \delta_d(r, r_o + r_w, r_{\boldsymbol{r}} + r_w)\big)\mathbb{P}(W_3(r_{\boldsymbol{r}}) \le W_4(r_w)) \\ + \delta_d(r, r_o + r_w, r_{\boldsymbol{r}} + r_w)\mathbb{P}(W_1(r_o) \le W_2(r_w) \cup W_3(r_{\boldsymbol{r}}) \le W_4(r_w))\Big] \\ F_R(\mathrm{d}r_w)\Big\} F_R(\mathrm{d}r_{\boldsymbol{r}}) F_R(\mathrm{d}r_o).\end{aligned} \tag{13}$$

Proof Consider two points, one at the origin, o, and the other at a distance r from the origin, in location $\boldsymbol{r}$. As before, use $\mathcal{M}_{o,\boldsymbol{r}}(m_o = 1, m_{\boldsymbol{r}} = 1)$ in (5) and condition on the sphere at o having radius r_o and the sphere at $\boldsymbol{r}$ having radius $r_{\boldsymbol{r}}$. Denote a point in x having radius r_x by $[x; r_x]$. If the distance between o and $\boldsymbol{r}$ is less than the sum of their radii, both of the points cannot be retained, hence we integrate over all radii such that $r > r_o + r_{\boldsymbol{r}}$

$$\begin{aligned}\mathcal{M}_{o,\boldsymbol{r}}(m_o = 1, m_{\boldsymbol{r}} = 1) = \int_0^\infty\int_0^\infty 1_{\{r>r_o+r_{\boldsymbol{r}}\}} \\ \mathbb{P}(\{\#\text{ points that win over } [o; r_o] \text{ or } [\boldsymbol{r}; r_{\boldsymbol{r}}]\} = 0) F_R(\mathrm{d}r_o) F_R(\mathrm{d}r_{\boldsymbol{r}}).\end{aligned} \tag{14}$$

As before, the points that win over $[o; r_o]$ or $[\boldsymbol{r}; r_{\boldsymbol{r}}]$ constitute an inhomogeneous Poisson process with intensity function $\lambda_b(x)$. When λ is the intensity of the stationary Poisson process, the mean number of points in $\mathbb{R}^d$ of this inhomogeneous process can be written

$$\begin{aligned}\int_{\mathbb{R}^d} \lambda_b(x)\mathrm{d}x = \int_{\mathbb{R}^d} \lambda \mathbb{P}(\text{A point in } x \text{ wins over } [o; r_o] \text{ or } [\boldsymbol{r}; r_{\boldsymbol{r}}])\mathrm{d}x \\ = \lambda \int_{\mathbb{R}^d}\int_0^\infty \mathbb{P}(\text{A point in } [x; r_w] \text{ wins over } [o; r_o] \text{ or } [\boldsymbol{r}; r_{\boldsymbol{r}}]) F_R(\mathrm{d}r_w)\mathrm{d}x.\end{aligned} \tag{15}$$

A point with radius r_w is a possible candidate for winning over o if it belongs to the set

$$\{x \in \mathbb{R}^d : B_d(o, r_o) \cap B_d(x, r_w) \neq \emptyset\} = B_d(o, r_o + r_w),$$

and similarly it is a candidate for winning over $\boldsymbol{r}$ if it belongs to $B_d(\boldsymbol{r}, r_w + r_{\boldsymbol{r}})$. Points in $B_d(o, r_o + r_w) \cap B_d(\boldsymbol{r}, r_w + r_{\boldsymbol{r}})$ can win over both o and $\boldsymbol{r}$. These three sets can be made into three disjoint sets, and letting $W_i(x)$ have distribution $F_{W|x}$, we get

$$\begin{aligned}&\int_{\mathbb{R}^d} \lambda_b(x)\mathrm{d}x \\ &=\lambda \int_{\mathbb{R}^d}\int_0^\infty \Big[1_{\{B_d(o,r_o+r_w)\setminus B_d(\boldsymbol{r},r_{\boldsymbol{r}}+r_w)\}}(x)\mathbb{P}(W_{x1}(r_w) \geq W_o(r_o)) \\ &+1_{\{B_d(\boldsymbol{r},r_{\boldsymbol{r}}+r_w)\setminus B_d(o,r_o+r_w)\}}(x)\mathbb{P}(W_{x2}(r_w) \geq W_{\boldsymbol{r}}(r_{\boldsymbol{r}})) \\ &+1_{\{B_d(\boldsymbol{r},r_{\boldsymbol{r}}+r_w)\cap B_d(o,r_o+r_w)\}}(x)\mathbb{P}(W_{x1}(r_w) \geq W_o(r_o) \cup W_{x2}(r_w) \geq W_{\boldsymbol{r}}(r_{\boldsymbol{r}}))\Big] \\ &\quad F_R(\mathrm{d}r_w)\mathrm{d}x.\end{aligned}$$

The weights do not depend on x, thus giving,

$$\begin{aligned}
&\int_{\mathbb{R}^d} \lambda_b(x)\mathrm{d}x \\
&=\lambda \int \big[l_d(B_d(o, r_o + r_w) \setminus B_d(\boldsymbol{r}, r_{\boldsymbol{r}} + r_w))\mathbb{P}(W_{x1}(r_w) \geq W_o(r_o)) \\
&\quad + l_d(B_d(\boldsymbol{r}, r_{\boldsymbol{r}} + r_w) \setminus B_d(o, r_o + r_w))\mathbb{P}(W_{x2}(r_w) \geq W_{\boldsymbol{r}}(r_{\boldsymbol{r}})) \\
&\quad + l_d(B_d(\boldsymbol{r}, r_{\boldsymbol{r}} + r_w) \cap B_d(o, r_o + r_w)) \\
&\quad \mathbb{P}(W_{x1}(r_w) \geq W_o(r_o) \cup W_{x2}(r_w) \geq W_{\boldsymbol{r}}(r_{\boldsymbol{r}}))\big] F_R(\mathrm{d}r_w).
\end{aligned} \tag{16}$$

The probability in (14) is

$$\begin{aligned}
&P_b(\{\#\text{ of points that win over } [o; r_o] \text{ or } [\boldsymbol{r}; r_{\boldsymbol{r}}]\} = 0) \\
&\quad = \exp\Big\{ -\int_{\mathbb{R}^d} \lambda_b(x)\mathrm{d}x \Big\}.
\end{aligned} \tag{17}$$

Insert (16) and (17) in (14), multiply by λ^2 and the proof is completed. □

Theorem 5 *Let $\delta_d(r, r_o + r_w, r_{\boldsymbol{r}} + r_w) = l_d(B_d(o, r_o + r_w) \cap B_d(\boldsymbol{r}, r_{\boldsymbol{r}} + r_w))$ with $|o - \boldsymbol{r}| = r$. With global assignment of weights the second-order product density is*

$$\begin{aligned}
\varrho^{(2)}(r) =& \lambda^2 \int_0^r \int_0^{r - r_o} \iint \exp\Big\{ -\lambda \int \\
&\Big[\int_{w_o}^{\infty} (\kappa_d(r_o + r_w)^d - \delta_d(r, r_o + r_w, r_{\boldsymbol{r}} + r_w)) F_{W|r_w}(\mathrm{d}w) \\
&+ \int_{w_{\boldsymbol{r}}}^{\infty} (\kappa_d(r_{\boldsymbol{r}} + r_w)^d - \delta_d(r, r_o + r_w, r_{\boldsymbol{r}} + r_w)) F_{W|r_w}(\mathrm{d}w) \\
&+ \int_{min(w_o, w_{\boldsymbol{r}})}^{\infty} \delta_d(r, r_o + r_w, r_{\boldsymbol{r}} + r_w) F_{W|r_w}(\mathrm{d}w) \Big] \\
&F_R(\mathrm{d}r_w) \Big\} F_{W|r_o}(\mathrm{d}w_o) F_{W|r_{\boldsymbol{r}}}(\mathrm{d}w_{\boldsymbol{r}}) F_R(\mathrm{d}r_{\boldsymbol{r}}) F_R(\mathrm{d}r_o).
\end{aligned} \tag{18}$$

Proof A point in x with its associated radius and weight is denoted by $[x; r_x; w_x]$. The ideas of the proof are the same as for the proof of Theorem 4, but condition also on the weights of the two typical points in o and $\boldsymbol{r}$ being w_o and $w_{\boldsymbol{r}}$ respectively, i.e. (14) becomes

$$\begin{aligned}
\mathcal{M}_{o,\boldsymbol{r}}(m_o = 1, m_{\boldsymbol{r}} = 1) = &\int_0^{\infty} \int_0^{\infty} \iint 1_{\{r > r_o + r_{\boldsymbol{r}}\}} \\
&\mathbb{P}(\{\#\text{ of points that win over } [o; r_o; w_o] \text{ or } [\boldsymbol{r}; r_{\boldsymbol{r}}; w_{\boldsymbol{r}}]\} = 0) \\
&F_{W|r_o}(\mathrm{d}w_o) F_{W|r_{\boldsymbol{r}}}(\mathrm{d}w_{\boldsymbol{r}}) F_R(\mathrm{d}r_o) F_R(\mathrm{d}r_{\boldsymbol{r}}).
\end{aligned}$$

Furthermore, to calculate the expectation of the number of points that beat o or $\boldsymbol{r}$, we must also condition on the weight of x

$$
\begin{aligned}
&\int_{\mathbb{R}^d} \lambda_b(x)\mathrm{d}x \\
&\quad = \int_{\mathbb{R}^d} \lambda \mathbb{P}(\text{A point in } x \text{ wins over } [o; r_o; w_o] \text{ or } [\boldsymbol{r}; r_{\boldsymbol{r}}; w_{\boldsymbol{r}}])\mathrm{d}x \\
&\quad = \lambda \int_{\mathbb{R}^d} \iiint [1_{\{B_d(o,r_o+r_w)\setminus B_d(\boldsymbol{r},r_{\boldsymbol{r}}+r_w)\}}(x) 1_{\{w_x \geq w_o\}} \\
&\qquad + 1_{\{B_d(\boldsymbol{r},r_{\boldsymbol{r}}+r_w)\setminus B_d(o,r_o+r_w)\}}(x) 1_{\{w_x \geq w_{\boldsymbol{r}}\}} \\
&\qquad + 1_{\{B_d(\boldsymbol{r},r_{\boldsymbol{r}}+r_w)\cap B_d(o,r_o+r_w)\}}(x) 1_{\{w_x \geq min(w_{\boldsymbol{r}},w_o)\}}] \\
&\qquad F_{W|r_w}(\mathrm{d}w_x) F_R(\mathrm{d}r_w)\mathrm{d}x.
\end{aligned}
$$

The last steps are the same as those in the proof of Theorem 4. □

Remark: If the weight distribution is continuous and independent of the radius it does not matter which form it has.

To evaluate the product density for special cases it is usually necessary to do the integration numerically. Below is a simple example of when it is possible to calculate the product density exactly, as an illustration of its behaviour.

Example 1 Consider a model in $\mathbb{R}^2$ with two spheres of radius r_1 and r_2 and let p_i be the probability of a sphere having radius r_i. Let the weight distribution be uniform and independent of the radius. An expression for $\delta_2(r, r_i + r_k, r_j + r_k)$, the area of the intersection of two discs with radii $r_i + r_k$ and $r_j + r_k$ at distance r, can be found in Appendix A. Then, for the pairwise model, the intensity after thinning is

$$
\lambda_{thP} = \lambda \sum_{i=1}^{2} p_i \exp\left\{ -\lambda \frac{1}{2} \pi \big((r_i + r_1)^2 p_1 + (r_i + r_2)^2 p_2 \big) \right\},
$$

by (1) and (2). By (13), the product density is

$$
\begin{aligned}
\varrho_P^{(2)}(r) = &\lambda^2 \sum_{i=1}^{2} \sum_{j=1}^{2} 1_{\{r_i + r_j < r\}} \exp\Big\{ -\lambda \sum_{k=1}^{2} \Big[\frac{\pi}{2} \big((r_i + r_k)^2 + (r_j + r_k)^2 \big) \\
&- \frac{1}{4} \delta_2(r, r_i + r_k, r_j + r_k) \Big] p_k \Big\} p_j p_i.
\end{aligned}
$$

Let $V_i = \sum_{k=1}^{2} p_k \pi (r_i + r_k)^2$ and $q_{i,j}(r) = \sum_{k=1}^{2} p_k \delta_2(r, r_i + r_k, r_j + r_k)$. From (1), (3) and (18), the corresponding quantities for the global model are

$$\lambda_{thG} = \sum_{i=1}^{2} \frac{1 - \exp\left\{-\lambda\pi \sum_{j=1}^{2} (r_i + r_j)^2 p_j\right\}}{\pi \sum_{j=1}^{2} (r_i + r_j)^2 p_j} p_i$$

and

$$\begin{aligned}
\varrho_G^{(2)}(r) = &\sum_{i=1}^{2}\sum_{j=1}^{2} 1_{\{r_i + r_j < r\}} \Big\{ (V_i - q_{i,j}(r))(V_j - q_{i,j}(r))(V_i + V_j) \\
&+ V_i V_j (V_i + V_j - 2q_{i,j}(r)) \exp[-\lambda(V_i + V_j - q_{i,j}(r))] \\
&- V_i (V_i + V_j - q_{i,j}(r))(V_j - q_{i,j}(r)) \exp[-\lambda V_j] \\
&- V_j (V_i + V_j - q_{i,j}(r))(V_i - q_{i,j}(r)) \exp[-\lambda V_i] \Big\} \\
&/ \Big\{ V_i V_j (V_i - q_{i,j}(r))(V_j - q_{i,j}(r))(V_i + V_j - q_{i,j}(r)) \Big\} p_i p_j .
\end{aligned}$$

The pair correlation functions, $\varrho^{(2)}/\lambda_{th}^2$, for both models with parameters $r_1 = 0.2$, $r_2 = 0.1$, $p_1 = 0.5$ and $p_2 = 0.5$, are shown in Figure 6. A sphere has radius $r_1 = 0.2$ with probability $p_1 = 0.5$ and radius $r_2 = 0.1$ with probability $p_2 = 0.5$. In the global model after thinning, the probability that a sphere has radius r_1 is approximately 0.58. In the pairwise model after thinning, the probability that a sphere has radius r_1 is approximately 0.72. The calculations of these probabilities can be done using Theorem 3.2 in [3]. The jump at $r = 0.2$ occurs because the spheres must have a radius which is at least 0.1 and consequently the points must be separated by at least 0.2. The next jump at $r = 0.3$ occurs because two spheres with radii which are 0.1 and 0.2, respectively, cannot be closer than 0.3. The final jump at $r = 0.4$ is explained in the same way.

6 Convex, compact grains

Let us instead of spherical grains consider grains with the same shape and orientation as a convex, compact set in $\mathbb{R}^d$. To describe such a set some notation is needed. For a set $A \subseteq \mathbb{R}^d$, the translation of A by $x \in \mathbb{R}^d$ is defined as

$$A_x = \{x + y : y \in A\},$$

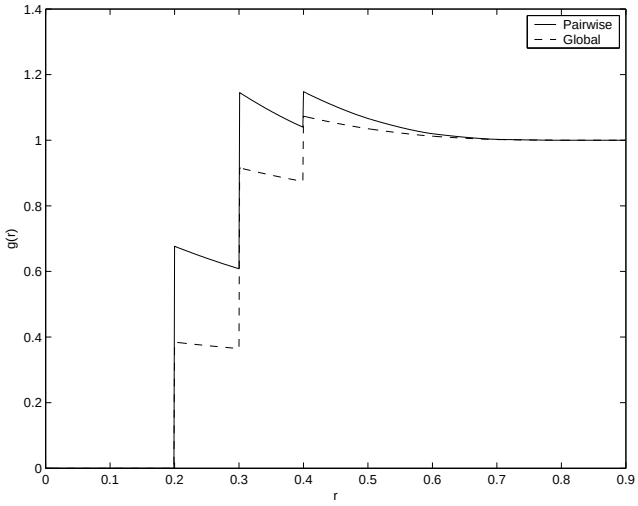

Figure 6: Pair-correlation function for the pairwise and the global model for spheres of two sizes with the same intensity after thinning, $\lambda_{th} = 2.5$.

the reflection of A is defined as

$$\check{A} = \{-x : x \in A\}$$

and the Minkowski-addition of A and $B \subseteq \mathbb{R}^d$ is defined as

$$A \oplus B = \{x + y : x \in A, y \in B\}.$$

Another useful way to write the Minkowski-addition is

$$A \oplus B = \{x : A \cap (\check{B})_x \neq \emptyset\}. \tag{19}$$

Define the size of a set $A \in \mathbb{R}^d$ as half its diameter, to have the size of a sphere equal to its radius, i.e. the size is defined as,

$$\frac{1}{2} \sup_{x,y \in A} |x - y|.$$

The family of convex, compact sets C in $\mathbb{R}^d$ having size 1 and containing the origin is denoted by $\mathcal{C}^d$. For $C \in \mathcal{C}^d$, let $C(r) = \{ry : y \in C\}$, that is a set of the same shape and orientation as C but of size $r > 0$. By Theorem 4.1 in [3], (2) and (3) are valid if $\kappa_d(r + y)^d$ is replaced by $\{x : l_d\{C(r) \cap C(y)_x \neq \emptyset\}$, or equivalently $l_d(C(r) \oplus \check{C}(y))$. For example,

the intensities for the thinned processes where all grains have the same size r_0, the intensity of the Poisson process before thinning is λ and the weight distribution is independent of size, are for the pairwise model,

$$\lambda_{thP} = \lambda \ \exp\left\{-\frac{1}{2}\lambda l_d\left(C(r_0) \oplus \check{C}(r_0)\right)\right\}$$

and for the global model,

$$\lambda_{thG} = \frac{1 - \exp\left\{-\lambda l_d\left(C(r_0) \oplus \check{C}(r_0)\right)\right\}}{l_d\left(C(r_0) \oplus \check{C}(r_0)\right)}.$$

The main difference from spheres is that the second-order product density cannot be written in terms of a distance anymore since the thinned process is not isotropic. However, the process is stationary, meaning that it is enough to consider $\varrho^{(2)}(o, y)$. The following notation is used in the theorems below. Let $Q(u, r_u, r) = l_d(C(r_u)_u \oplus \check{C}(r))$ and $S(o, r_o, y, r_y, r) = l_d((C(r_o) \oplus \check{C}(r)) \cap (C(r_y)_y \oplus \check{C}(r)))$.

Theorem 6 *With pairwise assignment of weights and convex grains with the same shape and orientation as $C \in \mathcal{C}^d$, the second-order product density is*

$$\begin{aligned}\varrho^{(2)}(o, y) = \lambda^2 \int_0^\infty \int_0^\infty 1_{\{r_o, r_y : C(r_o) \cap C(r_y)_y = \emptyset\}} \exp\Big\{-\lambda \int_0^\infty \\ \Big[\big(Q(o, r_o, r) - S(o, r_o, y, r_y, r)\big)\mathbb{P}(W_1(r_o) \le W_2(r)) \\ + \big(Q(y, r_y, r) - S(o, r_o, y, r_y, r)\big)\mathbb{P}(W_3(r_y) \le W_4(r)) \\ + S(o, r_o, y, r_y, r)\mathbb{P}(W_1(r_o) \le W_2(r) \cup W_3(r_y) \le W_4(r))\Big] \\ F_R(\mathrm{d}r)\Big\} F_R(\mathrm{d}r_o) F_R(\mathrm{d}r_y).\end{aligned} \tag{20}$$

Proof The proof is similar to that of Theorem 4. We consider one point at the origin and one point in y and want to find $\mathcal{M}_{o,y}(m_o = 1, m_y = 1)$. The integration corresponding to (14) is only done for sizes of the grains of o and y such that these grains are not overlapping, hence the indicator function in (14) is changed to $1_{\{r_o, r_y : C(r_o) \cap C(r_y)_y = \emptyset\}}$.

The only other difference compared with spherical grains is the sets where points can win over o or y. A point with a grain of size r is a possible candidate for winning over o if it belongs to the set

$$\{x \in \mathbb{R}^d : C(r_o) \cap C(r)_x \neq \emptyset\} = C(r_o) \oplus \check{C}(r),$$

where the equality comes from (19). Similarly a point in $C(r_y)_y \oplus \check{C}(r)$ can win over y. Points common to both these sets can win over either point, that is points in $(C(r_o) \oplus \check{C}(r)) \cap (C(r_y)_y \oplus \check{C}(r))$.

The remaining steps are the same as those in Theorem 4. □

Theorem 7 *With global assignment of weights and convex grains with the same shape and orientation as $C \in \mathcal{C}^d$, the second-order product density is*

$$\begin{aligned}\varrho^{(2)}(o,y) =& \lambda^2 \iiiint 1_{\{r_o,r_y:C(r_o)\cap C(r_y)_y=\emptyset\}} \exp\Big\{ -\lambda \int \\ & \Big[\int_{w_o}^{\infty} (Q(o,r_o,r) - S(o,r_o,y,r_y,r)) F_{W|r}(\mathrm{d}w) \\ & + \int_{w_y}^{\infty} (Q(y,r_y,r) - S(o,r_o,y,r_y,r)) F_{W|r}(\mathrm{d}w) \\ & + \int_{min(w_o,w_r)}^{\infty} S(o,r_o,y,r_y,r) F_{W|r}(\mathrm{d}w)\Big] \\ & F_R(\mathrm{d}r)\Big\} F_{W|r_o}(\mathrm{d}w_o) F_{W|r_y}(\mathrm{d}w_y) F_R(\mathrm{d}r_o) F_R(\mathrm{d}r_y).\end{aligned}$$

Proof Apply exactly the same modifications as in the proof above to the proof of Theorem 5. □

For ellipses and squares of equal sizes in $\mathbb{R}^d$, expressions for the Lebesgue-measures needed in this section are stated in Appendix A.

Example 2 For squares of equal size, in $\mathbb{R}^2$, the pair-correlation function is shown in Figure 7. As in Section 4.2 there are two pairwise models for one intensity after thinning. A discussion of the behaviour of the two models can be carried out in the same manner as in Section 4.2.

7 Concluding remarks

We have considered the second-order product density for two models of non-overlapping grains. In simple cases it is possible to get explicit results and in general we get integrals that need to be calculated numerically. It is an advantage of these models that they allow easy computation of the product density compared to many other models of non-overlapping grains found in literature.

As the models considered here were originally inspired by inclusions in cast iron it would be interesting to fit them to real data. We could try by using different radius distributions and change the way the weights depend on the radius.

Further future work could be to look at mark correlations of the thinned process, when the marks are the radii of the spheres, or in general the size of a convex set. Studying grains of different orientations could also be of interest.

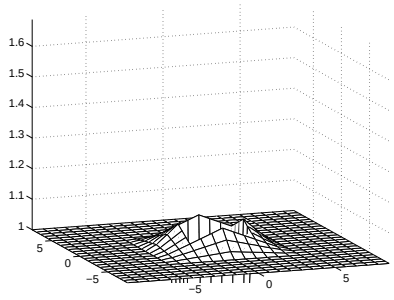

(a) Pairwise - low intensity before thinning

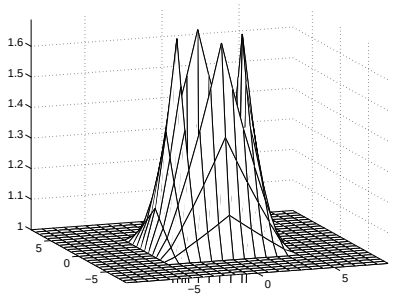

(b) Pairwise - high intensity before thinning

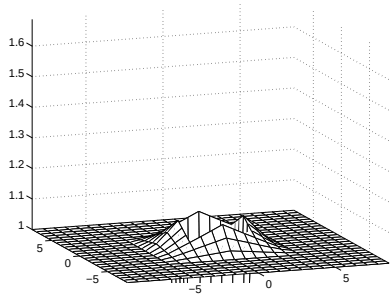

(c) Global

Figure 7: The pair-correlation function for squares of size $\sqrt{2}$, that is side of length 2, in two dimensions. The intensity after thinning is 0.03 for all three models. There are two pairwise models for one intensity after thinning, since the intensity after thinning behaves as in Figure 3. The pair-correlation is 0 for $-2 < x < 2$ and $-2 < y < 2$.

Acknowledgements

I would like to thank my supervisor, Marianne Månsson, for many helpful discussions and readings of this manuscript. I am also grateful for several valuable comments from my second supervisor, Jacques de Maré, during this work.

References

[1] Daley, D.J., Mallows, C.L., Shepp, L.A. (2000), *A one-dimensional Poisson growth model with non-overlapping intervals*. Stochastic Process. Appl., 90, 223-241.

[2] Jeulin, D. (1998), *Probabilistic models of structures*. PROBAMAT-21st century: probabilities and materials. Ed.G.N. Frantziskonis, Kluwer, Dordrecht, 233-257.

[3] Månsson, M., Rudemo, M. (2002), *Random patterns of nonoverlapping convex grains*. Adv. Appl. Prob., 34, 718-738.

[4] Matérn, B. (1960), *Spatial Variation*. Meddelanden Statens Skogsforskningsinst. 49. Statens Skogsforskningsinstitut, Stockholm, Second edition: Springer, Berlin, 1986.

[5] Stoyan, D. (1984), *On correlations of marked point processes*. Math. Nachr., 116, 197-207.

[6] Stoyan, D. (1987), *Statistical analysis of spatial point processes: a soft-core model and cross-correlations of marks*. Biom. J., 29, 971-980.

[7] Stoyan, D. (1988), *Thinnings of point processes and their use in the statistical analysis of a settlement pattern with deserted villages*. Statistics, 19, 45-56.

[8] Stoyan, D. (1990), *Stereological formulae for a random system of non-intersecting spheres*. Statistics, 21, 131-136.

[9] Stoyan, D. (1998), *Models of random systems of non-intersecting spheres*. Prague Stochastics '98, 543-547.

[10] Stoyan, D., Kendall, S.K., Mecke, J. (1995), *Stochastic Geometry and its Applications*. 2nd edition. Wiley.

[11] Stoyan, D. Penttinen, A. (2000), *Recent applications of point process methods in forestry statistics*. Statist. Sci., 15, 61-78.

[12] Stoyan, D. Schlather, M. (2000), *Random sequential adsorption: relationships to dead leaves and characterization of variability*. J. Statist. Phys., 100, 969-979.

[13] Stoyan, D. Stoyan, H. (1985), *On one of Matérn's hard-core point process models*. Math. Nachr., 122, 205-214.

[14] Talbot, J., Tarjus, G., Van Tassel, P.R., Viot, P. (2000), *From car parking to protein adsorption: an overview of sequential adsorption processes*. Colloids and Surfaces A, 165, 287-324.

A Areas and volumes for some convex sets

A.1 Sphere

d	$l_d(B_d(x,r))$	$l_d(B_d(x,h) \cap B_d(x+r,h))$
2	πr^2	$2h^2 \arccos \frac{r}{2h} - \frac{r}{2}\sqrt{4h^2 - r^2}$
3	$4/3\pi r^3$	$4/3\pi r^3 \left(1 - \frac{3r}{4h} + \frac{1}{16}\left(\frac{r}{h}\right)^3\right)$

$$\delta_2(r, r_1, r_2) = l_2(B_2(x, r_1) \cap B_2(x + r, r_2))$$
$$= r_1^2 \arccos\left(\frac{r^2 + r_1^2 - r_2^2}{2rr_1}\right) + r_2^2 \arccos\left(\frac{r^2 + r_2^2 - r_1^2}{2rr_2}\right)$$
$$- \frac{1}{2}\sqrt{2r^2r_1^2 + 2r^2r_2^2 + 2r_1^2r_2^2 - r^4 - r_1^4 - r_2^4}$$

A.2 Ellipse

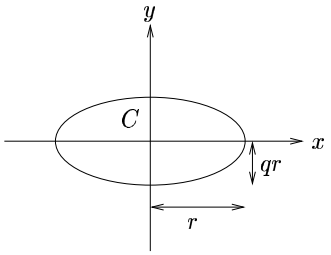

$$C(r) = \left\{(x, y) : \left(\frac{x}{r}\right)^2 + \left(\frac{y}{qr}\right)^2 \leq 1, 0 < q < 1\right\}$$

$$l_2(C(r)) = \pi q r^2$$

$$l_2(C(r) \oplus \check{C}(r)) = l_2(C(2r)) = 4\pi q r^2$$

The area of the intersection of two ellipses where the centre of the second ellipse is translated by $\boldsymbol{s} = (x_s, y_s)$ from the centre of the first is

$$l_2(C(r) \cap C(r)_{\boldsymbol{s}}) = q\, l_2(B_2(x, r) \cap B_2(x + \sqrt{x_s^2 + (y_s/q)^2}, r)).$$

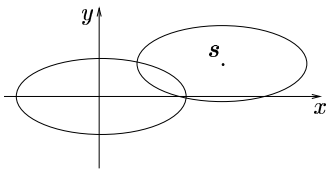

$$l_2([C(r) \oplus \check{C}(r)] \cap [C(r)_{\boldsymbol{s}} \oplus \check{C}(r)])$$
$$= q\, l_2(B_2(x, 2r) \cap B_2(x + \sqrt{x_s^2 + (y_s/q)^2}, 2r))$$

A.3 Square

$$C(r) = \left\{(x, y) : -r/\sqrt{2} \le x, y \le r/\sqrt{2}\right\}.$$

The area of the intersection of two squares where the centre of the second square is translated by $\boldsymbol{s} = (x_s, y_s)$ from the centre of the first is

$$l_2(C(r) \cap C(r)_{\boldsymbol{s}}) = |\sqrt{2}r - x_s| \cdot |\sqrt{2}r - y_s|.$$

$$l_2([C(r) \oplus \check{C}(r)] \cap [C_{\boldsymbol{s}}(r) \oplus \check{C}(r)]) = |2\sqrt{2}r - x_s| \cdot |2\sqrt{2}r - y_s|$$